ANALYSIS OF MIXING TANK

BE MECHANICAL ENGINEERING

By

Tayyeb Juned Momin (40)

Jayant Gangadhar Dhuri (10)

Masab Asif Selia (64)

Gaurang Milind Thakur (84)

Under the guide

MR. MANISH RANE

Shree Rahul Education Society's (Regd.)

SHREE L.R. TIWARICOLLEGE OF ENGINEERING, MIRA ROAD

(Approved by AICTE, Govt. of Maharashtra & Affiliated to University of Mumbai)

DEPARTMENT OF MECHANICAL ENGINEERING

2022-2023

A Project Report

On

ANALYSIS OF MIXING TANK

Submitted in fulfilment of the requirement for the course in

BE MECHANICAL ENGINEERING

By

Tayyeb Juned Momin (40)

Jayant Gangadhar Dhuri (10)

Masab Asif Selia (64)

Gaurang Milind Thakur (84)

Shree Rahul Education Society's (Regd.)

SHREE L.R. TIWARICOLLEGE OF ENGINEERING, MIRA ROAD

(Approved by AICTE, Govt. of Maharashtra & Affiliated to University of Mumbai)

DEPARTMENT OF MECHANICAL ENGINEERING

2022-2023

Shree Rahul Education Society's (Regd.)

SHREE L.R. TIWARICOLLEGE OF ENGINEERING, MIRA ROAD

(Approved by AICTE, Govt. of Maharashtra & Affiliated to University of Mumbai)

CERTIFICATE

This is to certify that the project titled **"ANALYSIS OF MIXING TANK"** Has been completed under our supervision and guidance by the following students**:**

Tayyeb Juned Momin (40)

Jayant Gangadhar Dhuri (10)

Masab Asif Selia (64)

Gaurang Milind Thakur (84)

In fulfilment of the requirement for the course in Fourth Year in Mechanical Engineering, as prescribed by University of Mumbai during the Academic Year 2022 – 2023. The said work has been assessed and is found to be satisfactory.

Mr. Manish Rane

Project Guide

Mr. Manish Rane

HOD

Dr. Deven Shah

Principal

CERTIFICATE

This is to certify that Analysis of Mixing Tank has been completed successfully and submitted by

Tayyeb Juned Momin (40)

Jayant Gangadhar Dhuri (10)

Masab Asif Selia (64)

Gaurang Milind Thakur (84)

Students of Mechanical Engineering, as prescribed by University of Mumbai in partial fulfilment of requirement for degree in Bachelor of Engineering (Mechanical) during the academic year of 2022 – 2023.

Internal Guide	External Examiner	Project Convener
Mr. Manish Rane	_____	Mr. Durgesh Pal

HOD	Principal
Mr. Manish Rane	Dr. Deven Shah

CERTIFICATE OF APPROVAL

Project Entitled:

Analysis of Mixing Tank

Submitted by:

Tayyeb Juned Momin (40)

Jayant Gangadhar Dhuri (10)

Masab Asif Selia (64)

Gaurang Milind Thakur (84)

In fulfilment of the requirement for the course in Fourth Year in "Mechanical Engineering" is approved.

Examiner(s):

Internal: Mr. Manish Rane

External:

Declaration by the Candidate

I/We declare that this written submission represents my ideas in my own words and where others' ideas or words have been included, I/We have adequately cited and referenced the original sources. I/We also declare that I/We have adhered to all principles of academic honesty and integrity and have not misrepresented or fabricated or falsified any idea/data/fact/source in my submission. I/We understand that any violation of the above will be cause for disciplinary action by the Institute and can also evoke penal action from the sources which have thus not been properly cited or from whom proper permission has not been taken when needed.

Date: 3rd May, 2023

(Tayyeb Juned Momin)

Roll No.: 40 Exam. Seat No.:

(Jayant Gangadhar Dhuri)

Roll No.: 10 Exam. Seat No.:

(Masab Asif Selia)

Roll No.: 64 Exam. Seat No.:

(Gaurang Milind Thakur)

Roll No.: 84 Exam. Seat No.:

Acknowledgement

We would like to express our heartfelt gratitude and respect to all those who have provided us with immense help and guidance throughout our project. Firstly, we would like to thank our Project Guide and Head of Department, Prof. Manish Rane, for providing us with a clear vision about the system and offering us regular critical reviews and inspiration throughout our work. We are grateful for their guidance, encouragement, understanding, and insightful support during the development process. We would also like to extend our thanks to our college for providing us with the necessary resources whenever we needed them and for giving us the opportunity to develop the project. We would like to express our sincere appreciation to our Principal, Dr. Devan Shah, for facilitating us with essential infrastructure and resources, without which this project would not have been possible.

Additionally, we are thankful to the entire staff of the Mechanical Department for their constant encouragement, suggestions, and moral support throughout the project's duration. We would also like to acknowledge and extend our gratitude to our friends and all those who have been associated with our project at any stage but whose names do not find a place in this acknowledgement. We are greatly indebted to each and every one for their contribution towards our project's success.

(Tayyeb Juned Momin)

Roll No.: 40 Exam. Seat No.:

(Jayant Gangadhar Dhuri)

Roll No.: 10 Exam. Seat No.:

(Masab Asif Selia)

Roll No.: 64 Exam. Seat No.:

(Gaurang Milind Thakur)

Roll No.: 84 Exam. Seat No.:

Abstract

Mixing is a crucial process in various industries, including pharmaceuticals, chemicals, and food, where the homogeneous mixing of two or more substances with the highest quality is essential. However, achieving a homogeneous mixture can be challenging as the efficiency of the mixing tank can be severely impacted by the formation of dead zones during the mixing process. Dead zones occur due to the particular fluid flow pattern generated by the impellers, which can cause improper mixing.

To eliminate the dead zones and ensure optimal mixing quality, we propose a solution that involves positioning and orienting the impeller to disrupt the flow pattern. The optimal impeller position will be determined through Computational Fluid Dynamics (CFD) analysis, which will induce additional turbulence in the system. In this study, we plan to use various sensors such as temperature sensors or electricity conductive probes to detect the potential dead zones and motors to adjust the impeller's position.

The data collected by the sensors will be analyzed to optimize the impeller's positioning and reduce the mixing time. The proposed approach not only reduces the mixing time but also improves the mixing quality. We expect to obtain a homogeneous mixture with minimal dead zones and ensure efficient mixing in a shorter time frame. Our approach will have significant implications for various industries that rely on optimal mixing quality for their products.

Overall, this study proposes a novel solution to eliminate dead zones in mixing tanks and optimize mixing quality, using CFD analysis to determine the optimal impeller position. We expect our approach to have practical applications in various industries and help improve their efficiency and product quality.

Table of Contents

CERTIFICATE iii
CERTIFICATE iv
CERTIFICATE OF APPROVAL v
Declaration by the Candidate vi
Acknowledgement vii
Abstract viii
1. Introduction 1
1.1. Scope of the project 2
1.2. Goals 2
1.3. Definition of mixing quality 2
1.3.1. Intensity of segregation 3
1.3.2. Multidimensional definition of segregation 4
1.4. Definitions of the mixing time – uniformity criteria 5
1.5. Experimental techniques for determination of the mixing time 6
1.6. Mathematical models for prediction of the mixing time 7
2. Theory 8
2.1. Introduction 8
2.2. Pre-processor 9
2.3. Solver 9
2.4. Post processor 10
2.5. Governing Differential Equations 11
2.6. Modeling Turbulence 12
2.7. Large eddy simulation: 13
2.8. Reynolds-averaged Navier–Stokes (RANS) equations: 13
2.9. Direct numerical simulation (DNS): 13
2.10. Reynolds-averaged Navier–Stokes (RANS) equations 14
2.11. RANS based Turbulence model 16
2.12. k-Epsilon model 16
2.13. Realizable k-Epsilon model 17
2.14. k-ω model 17
2.15. Species Transport 18
2.16. Multiple reference frame 18
2.17. Sliding mesh 20

2.18. SIMPLE Algorithm 21
2.19. Convergence 21
3. Literature Review 24
4. Methodology 26
4.1. Geometry model 26
4.2. Mesh 28
4.3. Boundary conditions 29
4.4. Solver settings 30
4.5. Stopping criteria 31
4.6. Post-processing 32
5. Result And Discussion 34
5.1. Flow Fields 34
5.2. Setting up velocity 34
5.3. Mixing Time 35
5.4. Correlation between mixing time and impeller type 47
5.5. Correlation between mixing time and blade angle 51
5.6. Correlation between mixing time and shaft clearance 51
6. Conclusion 52
7. Future Work 53
8. Bibliography 57

List of Figures

1.1: The concept of segregation 3
1.2: Time-variant turbulent fluctuations of concentration (C'A) about a mean value 3
2.1 CFD simulation of mixing tank 8
2.2 Different methods of turbulence modelling 12
2.3 Decomposition of instantaneous velocity 14
2.4 Triple decomposition for URANS method 15
2.5 Moving Reference Frame 19
2.6 Sliding mesh approach 20
2.7 Flow process of SIMPLE algorithm 22
4.1: Model used with the interface separating the two designated regions for unbaffled and baffled configuration. 26
4.2: Radial impeller detailed geometry 27
4.3: Propeller impeller detailed geometry 27
4.4: Inclined impeller detailed geometry 28
4.5: Mesh Used 28
4.6: Probes for Post processing 32
4.7: Tracer region 33
5.1: Convergence 34
5.2: Radial Impeller Baffled @ 300 RPM 35
5.3: Radial Impeller Unbaffled @ 300 RPM 35
5.4: Inclined Impeller Baffled @ 300 RPM 36
5.5: Inclined Impeller Unbaffled @ 300 RPM 36
5.6: Propeller Impeller Baffled @ 300 RPM 37
5.7: Propeller Impeller Unbaffled @ 300 RPM 37
5.8: Radial Impeller Baffled @ 400 RPM 38
5.9: Radial Impeller Unbaffled @ 400 RPM 38
5.10: Inclined Impeller Baffled @ 400 RPM 39
5.11: Inclined Impeller Unbaffled @ 400 RPM 39
5.12: Propeller Impeller Baffled @ 400 RPM 40
5.13: Propeller Impeller Unbaffled @ 400 RPM 40
5.14: Radial Impeller Baffled @ 500 RPM 41
5.15: Radial Impeller Unbaffled @ 500 RPM 41
5.16: Inclined Impeller Baffled @ 500 RPM 42
5.17: Inclined Impeller Unbaffled @ 500 RPM 42
5.18: Propeller Impeller Baffled @ 500 RPM 43
5.19: Propeller Impeller Unbaffled @ 500 RPM 43
5.20: Radial Impeller Baffled @ 700 RPM 44
5.21: Radial Impeller Unbaffled @ 700 RPM 44
5.22: Inclined Impeller Baffled @ 700 RPM 45
5.23: Inclined Impeller Unbaffled @ 700 RPM 45
5.24: Propeller Impeller Baffled @ 700 RPM 46
5.25: Propeller Impeller Unbaffled @ 700 RPM 46
5.26: Concentration Radial Impeller Baffled 47
5.27: Concentration Radial Impeller Unbaffled 48
5.28: Concentration Inclined Impeller Baffled 48
5.29: Concentration Inclined Impeller Unbaffled 49
5.30: Concentration Propeller Impeller Baffled 50
5.31: Concentration Propeller Impeller Unbaffled 50

List of Tables

4.1: Measures of the tank	27
4.2: Boundary conditions of the model.	30
4.3: General models for the physics setup.	31
4.4: Stopping criteria set for the simulations.	31
5.1: Correlation between mixing time and blade angle	51
5.2: Correlation between mixing time and shaft clearance	51

1. Introduction

Mixing tanks play a critical role in a wide range of process industries, such as chemical, pharmaceutical, food, oil and biochemical, as well as in municipal and industrial wastewater treatment plants. The efficiency of the mixing process can significantly impact product quality, energy consumption, and overall process economics. Thus, understanding the behaviour and performance of mixing tanks is of utmost importance in these industries.

The selection of tank geometry and impeller type depends on the purpose of the application carried out in the mixer, such as blending of miscible liquids, solid suspension, dispersion of gas into liquid, and heat and mass transfer enhancement, among others. The impeller design has a direct impact on the performance of mixing, and selecting the right impeller type and configuration is crucial to achieving optimal mixing efficiency.

Although significant progress has been made in the development of different impellers, there is still a lack of comprehensive understanding of the complex flow behaviour inside mixing tanks. The flow structure inside stirred tanks have been investigated using various flow measurement techniques, including laser Doppler anemometry (LDA), particle image velocimetry (PIV), and laser sheet illumination (LSI). While these experimental studies have provided valuable insights into the flow fields, the associated costs and practical limitations have restricted their widespread use.

To overcome these limitations, computational fluid dynamics (CFD) simulations have become increasingly popular in the investigation of flow behaviour inside stirred tanks. CFD tools allow for the study of the complex flow behaviour inside tanks and provide a cost-effective and practical alternative to experimental methods.

In this thesis, we aim to investigate the hydrodynamics of mixing tanks using CFD simulations. We will focus on understanding the impact of impeller geometry and turbulent models on the performance of mixing. Our goal is to develop a better understanding of the behaviour and performance of mixing tanks and provide recommendations for optimal design and operation.

In conclusion, this thesis is essential for industries that utilize mixing tanks and for researchers interested in understanding the hydrodynamics of mixing tanks. The results of this study will contribute to the optimization of mixing processes, leading to improved product quality, reduced energy consumption, and enhanced process economics.

1.1. Scope of the project

The aim of this report is to understand the effects of various impellers and tank configurations on the mixing time. The methodology used as the baseline is further described in the report.

Two different types of tank configurations were modelled, simulated and analysed. Both the tanks had the same volume. The first tank was not equipped with baffles, which are used as flow directing or obstructing panels used to direct the flow of fluid. The second tank was equipped with baffles to visualize the effect of baffles on the mixing time and mixing quality.

Apart from the two tank configurations, three different types of impellers were used and tested on four speeds. This helped to understand the changes in mixing time based on the impeller and tank configuration at different speeds.

1.2. Goals

The main goals of this project, based on the scope, are summarized in the following bullets points:

- Improved understanding of how the baffled and unbaffled configuration affects the mixing time and mixing quality.
- Improved understanding of how the different impellers affect the mixing time and mixing quality.
- Improved understanding of how the mixing time and mixing quality changes with respect to the speed.

1.3. Definition of mixing quality

Although a number of definitions of the mixing quality have been proposed in the literature, no single definition accurately and clearly describes the full range of problems in the field of industrial mixing. Some of the proposed approaches are reviewed.

1.3.1. Intensity of segregation

In chemical reactor engineering, the assumption is usually made that only the mean concentration needs to be considered; in reality, concentration values fluctuate about a mean, and in some cases these fluctuations must be considered in detail.[1] The concept of segregation and its meaning to chemical reactors was first described by Danckwerts.[2] The intensity of segregation is a measure of the difference in concentration between the purest concentration of component A and the purest concentration of component B in the surrounding fluid.[3] The intensity of segregation is a parameter that varies between one and zero, and is presented schematically in Figure 1.1.

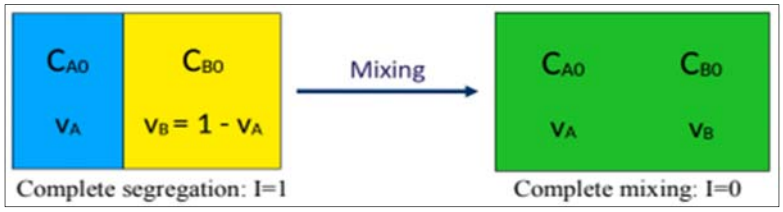

Figure 1.1 The concept of segregation [3]

The intensity of segregation can be described in terms of concentration fluctuations illustrated in Figure 1.2.

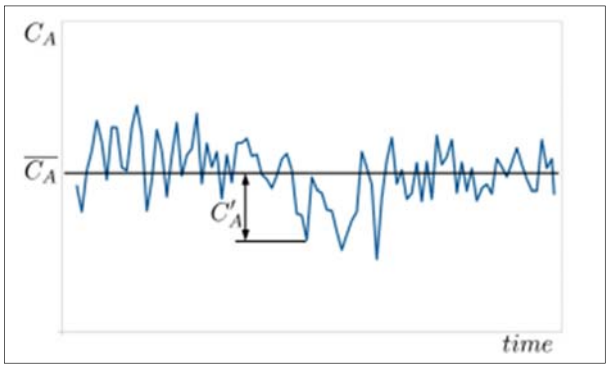

Figure 1.2 Time-variant turbulent fluctuations of concentration (C'A) about a mean value [3]

The unmixedness can be characterized by the mean of the square of the fluctuations or concentration variance:

$$\overline{C'_A{}^2} = \overline{(\overline{C_A} - C'_A)^2} \qquad (1.1)$$

To quantify the "state of unmixedness" Danckwerts introduced the concept of the intensity of segregation (I), which is calculated in terms of the mean square of the fluctuations [1], as:

$$I(t) = \frac{\overline{C'_A{}^2}}{\overline{C'_{A0}{}^2}} \tag{1.2}$$

where the subscript 0 denotes the initial or feed value. In a segregated system or in a system without a complete mixing, the rate of any reaction between the reactants would obviously be influenced by the rate of mixing, as measured by the change in I. Starting with the general macroscopic mass balance equation for segregation or unmixedness in a non-reactive batch reactor system where only the accumulation and dissipation terms are important [1], we get:

$$V\frac{d\overline{(C'_A{}^2)}}{dt} = -\frac{1}{\tau_m}\overline{C'_A{}^2}V \tag{1.3}$$

With the initial value $\overline{C'_{A0}{}^2}$ integration gives:

$$\frac{\overline{C'_A{}^2}}{\overline{C'_{A0}{}^2}} = I(t) = e^{-\frac{1}{\tau_m}} \tag{1.4}$$

where t is time elapsed in the process and τ_m is mixing time. This equation predicts that the intensity of segregation decays with time in the batch reactor. A similar equation can be derived for a steady-state plug flow system where the mean residence time should be used instead of t. [1] However, all non-idealities are lumped into a single parameter τ_m and therefore in this approach it is not possible to identify what is the source of
the non-idealities.

1.3.2. Multidimensional definition of segregation

Several mixing objectives occur simultaneously in a single application and can be grouped into three categories: (a) blending of miscible liquids, (b) multiphase mixing with at least one of several objectives: "just contacted", completely distributed throughout the vessel, size reduction, or mass transfer, and (c) reaction (homogeneous or heterogeneous).[4] The analysis of these applications reveals three variables directly related to mixing: (a) a reduction in the segregation of concentration, (b) a reduction in the scale of segregation, and (c) a mixing time scale. Consequently, Kukukova defined segregation as being composed of three separate dimensions: (i) the intensity of segregation quantified by the normalized concentration variance (concentration scale), (ii) the scale of segregation or clustering (length scale), and (iii) the exposure or the potential to reduce segregation (rate of change of segregation). The first dimension focuses on the instantaneous concentration variance; the second on the instantaneous length scales in the mixing field; and the third on the driving force for change, i.e., the mixing time scale, or the instantaneous rate of reduction in segregation. [4]

1.4. Definitions of the mixing time – uniformity criteria

Although the mixing time is widely used in process industries, there is no standard definition for it in the literature. Besides the reactor design and the operating conditions in it, the measured blend time also depends on the measurement locations, the size and the number of the probes, and the final condition of mixing. Although the mixing time is widely used in process industries, there is no standard definition for it in the literature. Besides the reactor design and the operating conditions in it, the measured blend time also depends on the measurement locations, the size and the number of the probes, and the final condition of mixing. Distelhoff measured blend times defined by 90% and 95% at different locations and found that τ_{m90} vary up to 27% and τ_{m95} vary up to 21% among the probes. They also reported that the variation at τ_{m99} is much smaller, less than 8%. Most of the reported blend times are the average of the measured data from a small number of probes. [5] Kramers used two probes, Grenville used three probes, and Khang and Levenspiel used 4 probes. [6][7][8] Although such averaged blend times can reflect certain characteristics of the mixing process in the tank, they cannot completely reveal spatial differences in mixing efficiency caused by the non-uniform flow distribution.

Bakker presented several ways to measure variations in concentration (for all measures, greater numbers indicate a greater variation with no upper bound): [9]

(a) Coefficient of variation (ratio between the standard deviation and the average concentration):

$$CoV = \frac{\sigma_c}{\bar{c}} \tag{1.5}$$

Where $\sigma = \sqrt{\frac{1}{N}\sum_{i=1}^{N}(c_i - \bar{c})^2}$ and $\bar{c} = \frac{1}{N}\sum_{i=1}^{N} c_i$

(b) Ratio between maximum and minimum concentrations:

$$\frac{c_{max}}{c_{min}} \tag{1.6}$$

(c) Largest deviation between the extremes in concentration and the average concentration:

$$\Delta_{max} = max(c_{max} - \bar{c}, \bar{c} - c_{min}) \tag{1.7}$$

Since there is a need to have an absolute measure of uniformity U that is ≤ 1 with 1 (or 100%) indicating perfect uniformity, Bakker proposed the following uniformity criteria: [9]

(a) Ratio between the minimum and maximum concentrations (bound between 0 and 1)

$$U_{min/max} = \frac{c_{min}}{c_{max}} \quad (1.8)$$

(b) Based on coefficient of variance CoV (not bound):

$$U_{CoV} = 1 - CoV \quad (1.9)$$

(c) Based on largest deviation from the average (not bound; conceptually closer to common experimental techniques):

$$U_{\Delta} = 1 - \frac{\Delta_{max}}{\bar{c}} \quad (1.10)$$

All the above-mentioned measures of uniformity indicate perfect uniformity at values of 1, are not bound between 0 and 1, and do not take initial conditions into account. In general, it is most useful to be able to predict the time it takes to reduce concentration variations by a certain amount. This can be done by scaling the largest deviation in mass fraction at time t by the largest deviation at time t=0.

$$U_t = 1 - \frac{\Delta_{max}(t)}{\Delta_{max}(t=0)} \quad (1.11)$$

1.5. Experimental techniques for determination of the mixing time

A comprehensive review of available experimental techniques and influence of various parameters has been given by Nere and Ghotli. [10] [11] Experimental determination of the mixing time involves adding a tracer input (usually a pulse input) at some location in the reactor and measuring the tracer concentration as a function of time. The tracer then distributes throughout the vessel, mixes with the fluid in the reactor, until the final uniform concentration is achieved. The mixing time is defined as the time required to achieve a certain degree of uniformity. The tracer used can be a chemical species (inert or reacting), an electrolyte, or a thermal species. The measurement method depends on the type of the tracer and over the past several years, different measurement techniques have been developed [11] such as: (i) visual, (ii) conductivity, (iii) thermal, (iv) electrical impedance/resistance tomography, (v) laser-induced fluorescence (LIF), (vi) liquid-crystal thermography, and (vii) computer tomography with coherent light.

In the literature review, laser induced fluorescence is used. The LIF is a spectroscopic method used for studying structure of molecules, detection of selective species and flow visualization and measurements.

The species to be examined is excited with a laser. The excited species will after some time, usually in the order of a few nanoseconds to microseconds, de-excite and emit light at a wavelength longer than the excitation wavelength. This process can be captured on a camera to assess the mixing characteristics. The mixing time is calculated as the time required for attaining a picture with uniform colour throughout. This technique offers the same advantages as those given by the visual techniques. In addition, the mixing process throughout the tank can be monitored clearly as a function of time. The disadvantage is that the LIF requires a transparent reactor, which is rarely the case on an industrial scale.

1.6. Mathematical models for prediction of the mixing time

The rate of mixing of the species often is the controlling factor for the quality of the final product. In general, the mixing process in a turbulent flow in a stirred tank can be divided into three transport processes that each act at a different range of length scales. At the largest scales, the fluid materials are convected around the reactor at a rate controlled by the mean flow velocity. At the intermediate scales, mixing of the materials is further enhanced by turbulent diffusion due to the turbulent fluctuation of eddies of all sizes. At the smallest scales, molecular diffusion smooths out any remaining concentration gradients. The characteristic mixing times associated with each of these three ranges of scales are different. Nere and Ghotli wrote an expanded review of mixing time models and divided them into five categories: (a) semi-empirical correlations based on experimental data, (b) models based on bulk flow, which assume that the process is controlled by the bulk or convective flow, (c) dispersion based models, (d) models that segregate the whole stirred vessel into a network of interconnected zones, and (e) CFD models.[10][11] The characteristics of those types of models were extensively discussed by Nere and Ghotli.[10][11] In this work the CFD approach has been adopted. CFD models can be considered as a further advancement of the network of zones models as the local flow structure is resolved using the basic transport equations and the analysis considers local convection, dispersion, and its variation throughout the stirred vessel.

After understanding the basics of mixing quality and the various methods for determining the mixing time experimentally and mathematically as well, we will move on to understand the subject of Computational Fluid Dynamics and fluid flow simulations.

2. Theory

Now we will try to understand what is Computational Fluid Dynamics; its importance; working which is, governed by differential equations and the concepts which enable us to carry out complex fluid flow simulations and study flow field and different transport phenomena.

2.1. Introduction

Computational fluid dynamics or CFD is the analysis of systems involving fluid flow, heat transfer and associated phenomena such as chemical reactions by means of computer-based simulation. The technique is very powerful and spans a wide range of industrial and non-industrial application areas.

Some examples are:

- aerodynamics of aircraft and vehicles: lift and drag
- hydrodynamics of ships
- power plant: combustion in internal combustion engines and gas turbines
- turbomachinery: flows inside rotating passages, diffusers, etc.
- electrical and electronic engineering: cooling of equipment including microcircuits
- chemical process engineering: mixing and separation, polymer moulding

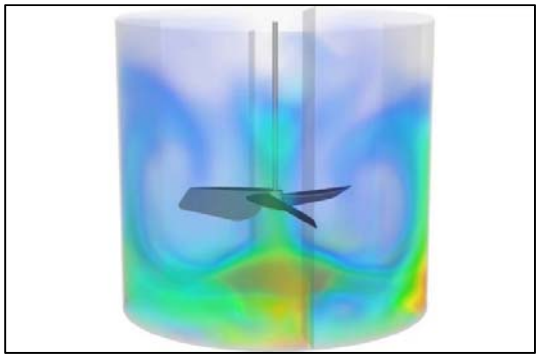

Figure 2.1 CFD simulation of mixing tank

CFD codes are structured around the numerical algorithms that can tackle fluid flow problems. In order to provide easy access to their solving power all commercial CFD packages include sophisticated user interfaces to input problem parameters and to examine the results. Hence, all codes contain three main elements:

- a pre-processor,

- a solver and
- a post-processor.

2.2. Pre-processor

Pre-processing consists of the input of a flow problem to a CFD program by means of an operator-friendly interface and the subsequent transformation of this input into a form suitable for use by the solver. The user activities at the pre-processing stage involve:

- Definition of the geometry of the region of interest: the computational domain
- Grid generation – the sub-division of the domain into a number of smaller, non-overlapping sub-domains: a grid (or mesh) of cells (or control volumes or elements)
- Selection of the physical and chemical phenomena that need to be modelled
- Definition of fluid properties
- Specification of appropriate boundary conditions at cells which coincide with or touch the domain boundary

The solution to a flow problem (velocity, pressure, temperature, etc.) is defined at nodes inside each cell. The accuracy of a CFD solution is governed by the number of cells in the grid. In general, the larger the number of cells, the better the solution accuracy. Both the accuracy of a solution and its cost in terms of necessary computer hardware and calculation time are dependent on the fineness of the grid. Optimal meshes are often non-uniform: finer in areas where large variations occur from point to point and coarser in regions with relatively little change. Efforts are underway to develop CFD codes with an (self-) adaptive meshing capability. Ultimately such programs will automatically refine the grid in areas of rapid variations. Up-to-date pre-processors also give the user access to libraries of material properties for common fluids and a facility to invoke special physical and chemical process models (e.g. turbulence models, radiative heat transfer, combustion models) alongside the main fluid flow equations.

2.3. Solver

There are three distinct streams of numerical solution techniques: finite difference, finite element and spectral methods. We shall be solely concerned with the finite volume method, a special finite difference formulation that is central to the most well-established CFD codes: CFX/ANSYS, FLUENT, PHOENICS and STAR-CD. In outline the numerical algorithm consists of the following steps:

- Integration of the governing equations of fluid flow over all the (finite) control volumes of the domain
- Discretisation – conversion of the resulting integral equations into a system of algebraic equations
- Solution of the algebraic equations by an iterative method

The first step, the control volume integration, distinguishes the finite volume method from all other CFD techniques. The resulting statements express the (exact) conservation of relevant properties for each finite size cell. This clear relationship between the numerical algorithm and the underlying physical conservation principle forms one of the main attractions of the finite volume method and makes its concepts much simpler to understand by engineers than the finite element and spectral methods. The conservation of a general flow variable φ, e.g., a velocity component or enthalpy, within a finite control volume can be expressed as a balance between the various processes tending to increase or decrease it.

In words we have:

$$\begin{bmatrix} Rate\ of\ change\ of\ \phi\ in\ the\ control\ volume\ with\ respect\ to\ time \end{bmatrix} = \begin{bmatrix} Net\ rate\ of\ increase\ of\ \phi\ due\ to\ convection\ into\ the\ control\ volume \end{bmatrix} + \begin{bmatrix} Net\ rate\ of\ increase\ of\ \phi\ due\ to\ diffusion\ into\ the\ control\ volume \end{bmatrix} + \begin{bmatrix} Net\ rate\ of\ creation\ of\ \phi\ inside\ the\ control\ volume \end{bmatrix}$$

CFD codes contain discretisation techniques suitable for the treatment of the key transport phenomena, convection (transport due to fluid flow) and diffusion (transport due to variations of φ from point to point) as well as for the source terms (associated with the creation or destruction of φ) and the rate of change with respect to time. The underlying physical phenomena are complex and non-linear, so an iterative solution approach is required. The most popular solution procedures are by the TDMA (tri-diagonal matrix algorithm) line-by-line solver of the algebraic equations and the SIMPLE algorithm to ensure correct linkage between pressure and velocity. Commercial codes may also give the user a selection of further, more recent, techniques such as Gauss–Seidel point iterative techniques with multigrid accelerators and conjugate gradient methods.

2.4. Post processor

As in pre-processing, a huge amount of development work has recently taken place in the post-processing field. Due to the increased popularity of engineering workstations, many of which have

outstanding graphics capabilities, the leading CFD packages are now equipped with versatile data visualisation tools. These include:

- Domain geometry and grid display
- Vector plots
- Line and shaded contour plots
- 2D and 3D surface plots
- Particle tracking
- View manipulation (translation, rotation, scaling etc.)
- Colour PostScript output

More recently these facilities may also include animation for dynamic result display, and in addition to graphics all codes produce trusty alphanumeric output and have data export facilities for further manipulation external to the code. As in many other branches of CAE, the graphics output capabilities of CFD codes have revolutionised the communication of ideas to the non-specialist. Typical decisions that might be needed are whether to model a problem in two or three dimensions, to exclude the effects of ambient temperature or pressure variations on the density of an air flow, to choose to solve the turbulent flow equations or to neglect the effects of small air bubbles dissolved in tap water. To make the right choices requires good modelling skills, because in all but the simplest problems we need to make assumptions to reduce the complexity to a manageable level whilst preserving the salient features of the problem at hand. It is the appropriateness of the simplifications introduced at this stage that at least partly governs the quality of the information generated by CFD, so the user must continually be aware of all the assumptions, clear-cut and tacit ones, that have been made.

2.5. Governing Differential Equations

All of CFD in one form or another, is based on the fundamental governing equations of fluid dynamics - the continuity equation, the momentum equation and energy equation. These equations speak physics.

The basics of CFD lie in solving fluid dynamics fundamental equations. These equations are nonlinear differential equations and serve as the basis for predicting the transient or steady state fluid flow.

They are the mathematical statements of three fundamental physical principles upon which all of fluid dynamics is based:

- Mass is conserved (Continuity equation):

$$\frac{\partial}{\partial t}\rho + \left(\frac{\partial}{\partial x_1}\rho u_1 + \frac{\partial}{\partial x_2}\rho u_2 + \frac{\partial}{\partial x_3}\rho u_3\right) = 0 \quad (2.1)$$

Equation (2.1) can be expressed in vector notation as:

$$\frac{\partial}{\partial t}\rho + \nabla \cdot \left(\rho \vec{V}\right) = 0 \quad (2.2)$$

If the fluid is incompressible (constant density) equations (2.1) and (2.2) will get converted into:

$$\left(\frac{\partial}{\partial x_1}u_1 + \frac{\partial}{\partial x_2}u_2 + \frac{\partial}{\partial x_3}u_3\right) = 0 \quad (2.3)$$

Equation (2.3) can be expressed in vector notation as:

$$\nabla \cdot \vec{V} = 0 \quad (2.4)$$

- Momentum is conserved (Momentum equation):

$$\frac{\partial}{\partial t}(\rho u_1) + \nabla\left(\rho u_1 \vec{V}\right) = -\frac{\partial}{\partial x_1}p + \nabla\left(\mu \frac{\partial}{\partial x_1}u_1\right) + S_{x_1} \quad (2.5)$$

$$\frac{\partial}{\partial t}(\rho u_2) + \nabla\left(\rho u_2 \vec{V}\right) = -\frac{\partial}{\partial x_2}p + \nabla\left(\mu \frac{\partial}{\partial y}u_2\right) + S_{x_2} \quad (2.6)$$

$$\frac{\partial}{\partial t}(\rho u_3) + \nabla\left(\rho u_3 \vec{V}\right) = -\frac{\partial}{\partial x_3}p + \nabla\left(\mu \frac{\partial}{\partial z}u_3\right) + S_{x_3} \quad (2.7)$$

The above equations can be represented in vector notation as:

$$\rho \frac{D\vec{V}}{Dt} = -\nabla p + \rho \vec{g} + \mu \nabla^2 \vec{V} \quad (2.8)$$

2.6. Modeling Turbulence

Turbulent flows are more difficult to describe since inertial forces are more dominant than viscous forces and big fluctuations cause the velocity and pressure fields to rapidly change.

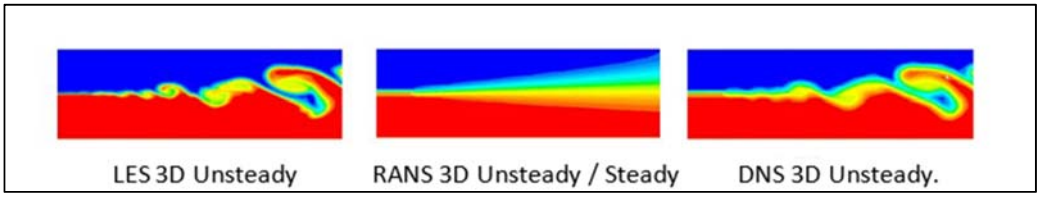

Figure 2.2 Different methods of turbulence modelling

Fluid flows in engineering applications are mostly turbulent, which requires that the whirls and vortices in the flow are resolved. There is always a question to what extend the flow needs to be resolved, which

will result in a more or less accurate solution. Turbulence causes the appearance in the flow of eddies with a wide range of length and time scales that interact in a dynamically complex way. Given the importance of the avoidance or promotion of turbulence in engineering applications, it is no surprise that a substantial amount of research effort is dedicated to the development of numerical methods to capture the important effects due to turbulence. The methods can be grouped into the following three categories:

2.7. Large eddy simulation:

This is an intermediate form of turbulence calculations which tracks the behaviour of the larger eddies. The method involves space filtering of the unsteady Navier–Stokes equations prior to the computations, which passes the larger eddies and rejects the smaller eddies. The effects on the resolved flow (mean flow plus large eddies) due to the smallest, unresolved eddies are included by means of a so-called sub-grid scale model. Unsteady flow equations must be solved, so the demands on computing resources in terms of storage and volume of calculations are large, but (at the time of writing) this technique is starting to address CFD problems with complex geometry.

2.8. Reynolds-averaged Navier–Stokes (RANS) equations:

The attention is focused on the mean flow and the effects of turbulence on mean flow properties. Prior to the application of numerical methods, the Navier–Stokes equations are time averaged (or ensemble averaged in flows with time-dependent boundary conditions). Extra terms appear in the time-averaged (or Reynolds averaged) flow equations due to the interactions between various turbulent fluctuations. These extra terms are modelled with classical turbulence models: among the best-known ones are the k–ε model and the Reynolds stress model. The computing resources required for reasonably accurate flow computations are modest, so this approach has been the mainstay of engineering flow calculations over the last three decades.

2.9. Direct numerical simulation (DNS):

These simulations compute the mean flow and all turbulent velocity fluctuations. The unsteady Navier–Stokes equations are solved on spatial grids that are sufficiently fine that they can resolve the Kolmogorov length scales at which energy dissipation takes place and with time steps sufficiently small to resolve the period of the fastest fluctuations. These calculations are highly costly in terms of computing resources, so the method is not used for industrial flow computations.

For most engineering purposes it is unnecessary to resolve the details of the turbulent fluctuations. CFD users are almost always satisfied with information about the time-averaged properties of the flow (e.g. mean velocities, mean pressures, mean stresses etc.). Therefore, the vast majority of turbulent flow computations has been and for the foreseeable future will continue to be carried out with procedures based on the Reynolds-averaged Navier–Stokes (RANS) equations.

2.10. Reynolds-averaged Navier–Stokes (RANS) equations

To make the problem possible to handle mathematically, the Navier-Stokes equations are often time-averaged. This idea uses the velocity decomposition concept into a mean and a fluctuating component.

$$\bar{u} = \frac{1}{T}\int_0^T u\, dt \tag{2.9}$$

The mean velocity of a turbulent flow can be defined as shown in the above equation. Therefore, the fluctuating component would be nothing but the difference between the total velocity and the mean (time-averaged) one. When deriving the time-averaged equations and decomposing the velocity in these two parts, it is also important to remember that, by definition, the mean of the fluctuating part is zero.

$$\mathrm{u} = \bar{\mathrm{u}} + u' \tag{2.10}$$

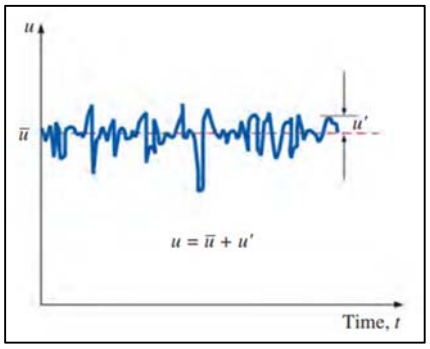

Figure 2.3 Decomposition of instantaneous velocity

Using then, the basic idea expressed in (2.10) and introducing it in Navier-Stokes equations (2.8), one derives the Reynolds Averaged Navier Stokes equations (RANS).

$$\frac{\partial u_1}{\partial t} + u_1\frac{\partial u_1}{\partial x_1} + u_2\frac{\partial u_1}{\partial x_2} + u_3\frac{\partial u_1}{\partial x_3}` = -\frac{1}{\rho}\frac{\partial P}{\partial x} + v\left(\frac{\partial^2 u_1}{\partial x_1^2} + \frac{\partial^2 u_1}{\partial x_2^2} + \frac{\partial^2 u_1}{\partial x_3^2}\right) + \frac{1}{\rho}\left[\frac{\partial\left(-\rho\overline{u_1'^2}\right)}{\partial x} + \frac{\partial\left(-\rho\overline{u_1'u_2'}\right)}{\partial y} + \frac{\partial\left(-\rho\overline{u_1'u_3'}\right)}{\partial z}\right] \tag{2.11}$$

$$\frac{\partial u_2}{\partial t} + u_1\frac{\partial u_2}{\partial x_1} + u_2\frac{\partial u_2}{\partial x_2} + u_3\frac{\partial u_2}{\partial x_3} = -\frac{1}{\rho}\frac{\partial P}{\partial y} + v\left(\frac{\partial^2 u_2}{\partial x_1^2} + \frac{\partial^2 u_2}{\partial x_2^2} + \frac{\partial^2 u_2}{\partial x_3^2}\right) + \frac{1}{\rho}\left[\frac{\partial\left(-\rho\overline{u_1' u_2'}\right)}{\partial x} + \frac{\partial\left(-\rho\overline{u_2'^2}\right)}{\partial y} + \frac{\partial\left(-\rho\overline{u_2' u_3'}\right)}{\partial z}\right] \quad (2.12)$$

$$\frac{\partial u_3}{\partial t} + u_1\frac{\partial u_3}{\partial x_1} + u_2\frac{\partial u_3}{\partial x_2} + u_3\frac{\partial u_3}{\partial x_3} = -\frac{1}{\rho}\frac{\partial P}{\partial z} + v\left(\frac{\partial^2 u_3}{\partial x_1^2} + \frac{\partial^2 u_3}{\partial x_2^2} + \frac{\partial^2 u_3}{\partial x_3^2}\right) + \frac{1}{\rho}\left[\frac{\partial\left(-\rho\overline{u_1' u_3'}\right)}{\partial x} + \frac{\partial\left(-\rho\overline{u_2' u_3'}\right)}{\partial y} + \frac{\partial\left(-\rho\overline{u_3'^2}\right)}{\partial z}\right] \quad (2.13)$$

The above equations can be expressed in vector form as:

$$\rho\frac{D\vec{V}}{Dt} = -\nabla P + \mu\nabla^2 + \nabla\cdot(-\rho\langle uu\rangle) \quad (2.14)$$

Due to the low computational resources needed by RANS models, the usage of them is widely spread through studies and researches. This is also increased based on the normal desire of the industry to obtain the mean behaviour of the flow, without having an interest in understanding what is happening on every turbulent scale. The vast majority of articles and industry works are carried using RANS models. However, they also have their drawbacks, mainly based on the turbulent viscosity hypothesis, that makes them unsuitable in various situations. In some occasions, a steady solution cannot be achieved when using RANS. This may be due to strong fluctuating or non-symmetrical flows. This can be resolved by using the time-accurate solution of the RANS equations, otherwise known as Unsteady RANS (URANS).

This is based on a triple decomposition of the time dependent variables. Each component of the decomposition is identified as average, periodic, and turbulent. When using this approach, the sum of time-average and periodic components (known as coherent or ensemble-averaged component) is solved

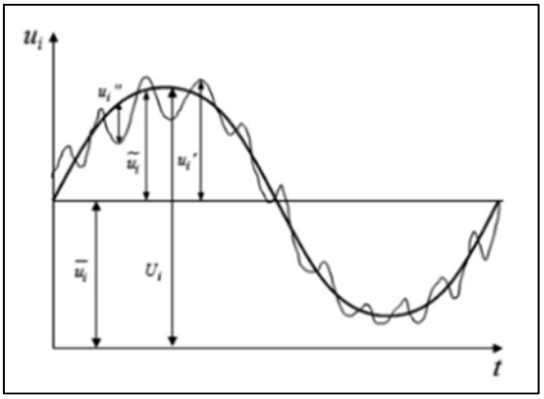

Figure 2.4 Triple decomposition for URANS method

using turbulence closure models. The turbulent component as before, is modelled. Discern between the periodic and turbulent components is normally, a cumbersome task. This is a clear issue of scale separation, that can lead to wrong component definitions and thus, wrong fluctuations being resolved.

$$u = \bar{u} + u' + u'' \tag{2.15}$$

2.11. RANS based Turbulence model

The turbulent viscosity appears as a turbulent diffusion coefficient for momentum when mimicking molecular diffusion. The RANS models, model this parameter in different ways. To obtain the turbulent viscosity, one could use an algebraic equation to approximate the value, a PDE or a set of PDEs to solve new transport equations for variables not yet seen. One good example of a 1-equation model would be the Spalart-Allmaras model, suitable for external aerodynamics applications. Among the 2-equation models, one can find the recognized $k-\varepsilon$ and the $k-\omega$ turbulence models.

2.12. k-Epsilon model

The k-epsilon model is a widely used turbulence model that has gained popularity due to its simplicity and computational efficiency. Despite its known limitations in complex flows involving severe pressure gradients, separation, and strong streamline curvature, the model remains a robust tool suitable for a variety of engineering applications. Its efficiency makes it an ideal choice for initial iterations, initial screening of alternative designs, and parametric studies.

Overall, while the k-epsilon model may not be suitable for all types of flows, it remains a powerful and widely used tool that provides valuable insights into turbulent flow behavior in many engineering applications.

The k-epsilon model has become one of the most widely used turbulence models due to its computational efficiency and relatively simple implementation. However, it has limitations in certain types of flows, particularly those with strong pressure gradients or near walls, where more advanced turbulence models may be required.

The k-epsilon model solves two additional transport equations for the turbulent kinetic energy (k) and its dissipation rate (epsilon) in order to provide closure for the RANS equations. The turbulent kinetic energy represents the energy associated with turbulent motion in the fluid, and the dissipation rate represents the rate at which this energy is dissipated due to viscous forces. By solving for these

quantities, the k-epsilon model is able to predict the effects of turbulence on the mean flow properties of a fluid.

k-transport equation-

$$\rho \frac{Dk}{Dt} = \frac{\partial}{\partial x_j}\left[\left(\mu + \frac{\mu_t}{\sigma_k}\right)\frac{\partial k}{\partial x_j}\right] + \mu_t S^2 - \rho\varepsilon \quad (16)$$

ε-transport equation-

$$\rho \frac{D\varepsilon}{Dt} = \frac{\partial}{\partial x_j}\left[\left(\mu + \frac{\mu_t}{\sigma_\varepsilon}\right)\frac{\partial \varepsilon}{\partial x_j}\right] + \frac{\varepsilon}{k}(C_1\mu_t S^2 - \rho C_{2\varepsilon}\varepsilon) \quad (17)$$

This 2-equation model assumes that the turbulent viscosity can be calculated as shown in the following equation:

$$\nu_T = \rho C_\mu \frac{k^2}{\varepsilon} \quad (18)$$

The equations also consist of some adjustable constants σ_k ,σ_ε, $C_{1\varepsilon}$ and $C_{2\varepsilon}$. The values of these constants have been arrived at by numerous iterations of data fitting for a wide range of turbulent flows. These are as follows:

$C\mu = 0.09$ $\sigma_k = 1.00$ $\sigma_\varepsilon = 1.30$ $C_{1\varepsilon} = 1.44$ $C_{2\varepsilon} = 1.92$

2.13. Realizable k-Epsilon model

The model differs from the original one mainly in the following ways:

- New turbulent viscosity formulation, that makes the parameter Cμ limited by a formula, instead of being a constant.
- New transport equation for the turbulent dissipation ε, derived from an exact transport equation for the mean-square vorticity fluctuation.

2.14. k-ω model

Being similar to the k−ε model, now the specific dissipation rate is the second transport equation solved. The specific dissipation rate is defined in equation (2.19). The new transport equation is shown in equation (2.20). This model was developed by Wilcox.

$$\omega = \frac{\varepsilon}{k} \quad (19)$$

$$\frac{\partial \omega}{\partial t} + \overline{u_j}\frac{\partial \omega}{\partial x_j} = C_{\omega 1}\frac{\omega}{k}P - C_{\omega 2}\omega^2 + \frac{\partial}{\partial x_j}\left[\left(\nu + \frac{\nu_T}{\sigma_\omega}\right)\right]\frac{\partial \omega}{\partial x_j} \quad (20)$$

This change makes the model better at handling vortices and it can also be used in the viscous sub-layer. Furthermore, it is also possible for it to handle adverse pressure gradients and the wall-boundary flow is well resolved if the case has a low Reynolds number. As a drawback, however, the model handles worse the freestream.

2.15. Species Transport

Species transport is a key aspect of CFD that involves modeling the transport and mixing of different chemical species within a fluid. This can be important in a range of applications, including combustion, chemical reactors, and environmental transport.

In CFD simulations, species transport is typically modeled using the advection-diffusion equation, which describes the transport of a species due to both advection (the bulk flow of the fluid) and diffusion (the random motion of the species due to concentration gradients). The equation can be further modified to account for chemical reactions, which may be important in some applications.

The advection-diffusion equation is solved using numerical techniques, such as finite volume or finite element methods, and requires the specification of boundary conditions at the inlet and outlet of the computational domain. The species transport equation is often coupled with other equations, such as the Navier-Stokes equations for fluid motion or the energy equation for heat transfer, to provide a comprehensive description of the physical system.

Species transport models can be complex, and accurate simulations require detailed information on the properties of the species being transported, such as diffusivity, reaction rates, and thermodynamic properties. However, the ability to model species transport is critical for understanding and predicting the behavior of many important physical processes in engineering and science, including combustion, chemical reactions, and atmospheric transport.

2.16. Multiple Reference Frame (MRF)

The Moving Reference Frame (MRF) approach is a commonly used technique in computational fluid dynamics (CFD) to model the flow field in rotating or moving geometries. The MRF approach involves transforming the computational domain into a reference frame that moves or rotates with the object of interest, such as a rotating propeller or turbine blade.

In the MRF approach, the fluid velocity and pressure are decomposed into two components: one in the moving reference frame and another in the stationary reference frame. The governing equations of fluid motion are then solved in the moving reference frame, where the equations are simpler due to the absence of the rotational or translational effects.

The MRF approach has several advantages, including reduced computational cost and improved numerical stability, compared to more complex techniques like overset grids or sliding mesh methods. The MRF approach is also relatively easy to implement and can provide accurate results for many engineering applications, including turbomachinery and wind turbine simulations.

However, the MRF approach has limitations, particularly in cases where the rotational effects are significant or where the flow is highly unsteady. In such cases, more advanced techniques may be required, such as the sliding mesh method or the immersed boundary method. Additionally, care must be taken when applying the MRF approach to ensure that the rotating or moving object is correctly represented, as errors in the object's motion can lead to inaccurate predictions of the flow field.

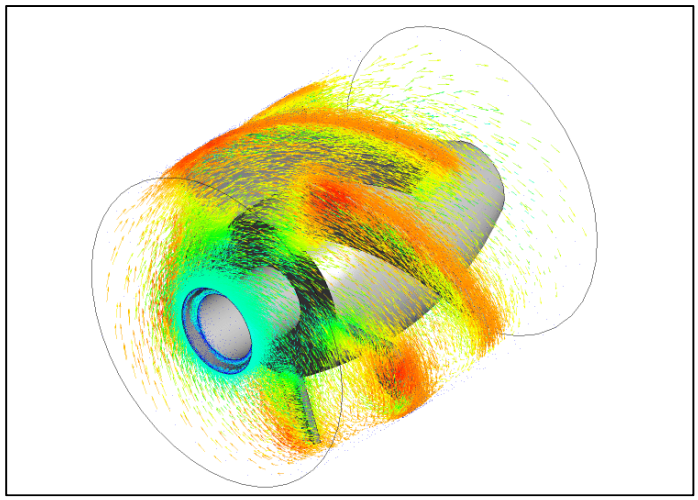

Figure 2.5 Moving Reference Frame

This approach applies a rotating reference frame to the spinning region. Based on it, a source term is added to each cell in the rotating domain. This source term simulates the rotation in the region, and that effect is propagated through the interface to the stationary region, transforming the local values from one frame to the other on a cell-by-cell basis. One must remark that in this approach, the mesh is completely frozen. As the mesh is not moving, the position of the stirrer blades with respect to the stationary walls remains unchanged. Therefore, the result obtained with MRF is dependent on the original position of the imported geometry. Different initial positions may lead to different final

snapshots of the solution, being one of the major drawbacks of the methodology. The MRF approach assumes that the volume assigned to the spinning domain has a constant rotational speed. By not having mesh motion, the steady state solution linked to that position of the stirrer can be computed. This makes the approach computationally cheap and, despite the limitations, accurate for several industrial problems. One big limitation is that, since the source term is added to every cell within the spinning region, no stationary walls can be located inside it. It can be used in baffled tanks, if the stationary domain can contain the baffles maintaining a good separation of the regions. The accuracy with MRF then, depends strongly on the impeller type and geometry.

2.17. Sliding mesh

The sliding mesh model is theoretically the most accurate method for simulating rotating flows and it is able to correctly describe the whole transient start up, but it is also the most computationally demanding. This technique, applied to the specific case, results in two cell zones that are created separately (the first one is a cylindrical cell containing the gear, the second one is the remaining volume). Each cell zone is bounded by an interface where it meets the opposing cell zone. The two cell zones will slide relative to one another along the mesh interface in discrete steps.

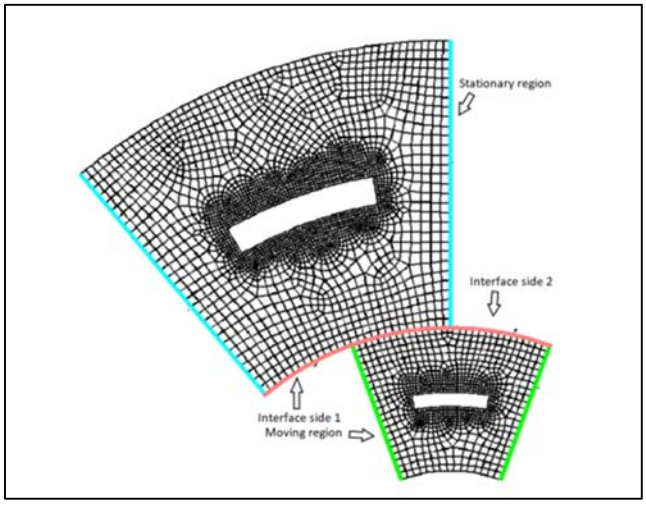

Figure 2.6 Sliding mesh approach.

The AMI (arbitrary mesh interface) operates by projecting one of the patches geometry onto the other. In other words, the two sub-domains are geometrically separated but numerically connected by the AMI that ensures that the values of a generic field are the same on both sides of the interface. The external

cell is a simple steady partition which mesh does not move during the calculations. The internal partition instead, the cylindrical one, is a cell zone that rotates during the simulations. After each time step, in fact, the internal mesh is rotated of a prescribed angle and, consequently, also the motion of the gear faces is in this manner correctly reproduced. The advantage of this technique, is that it ensures the best accuracy avoiding, at the same time, mesh deformation (that means an additional computational effort).

2.18. SIMPLE Algorithm

The acronym SIMPLE stands for Semi-Implicit Method for Pressure Linked Equations. The algorithm was originally put forward by Patankar and Spalding (1972) and is essentially a guess-and-correct procedure for the calculation of pressure on the staggered grid arrangement. On a staggered grid the scalar variables (pressure, density, total enthalpy etc.) are stored in the cell centres of the control volumes, whereas the velocity or momentum variables are located at the cell faces. This is different from a collocated grid arrangement, where all variables are stored in the same positions. A staggered storage is mainly used on structured grids for compressible or incompressible flow simulations. Using a staggered grid is a simple way to avoid odd-even decoupling between the pressure and velocity. Odd-even decoupling is a discretization error that can occur on collocated grids and which leads to checkerboard patterns in the solutions. The disadvantage of using staggered grids is that different variable is stored at different places and this makes it more difficult to handle different control volumes for different variables and to keep track of the metrics. Most modern codes instead use a collocated storage. The SIMPLE algorithm gives a method of calculating pressure and velocities. The method is iterative, and when other scalars are coupled to the momentum equations the calculation needs to be done sequentially. The process used in SIMPLE algorithm can be seen in Figure 2.7

2.19. Convergence

When the flow is aligned with the mesh (e.g., laminar flow in a rectangular duct modelled with a quadrilateral or hexahedral mesh) the first-order upwind discretization may be acceptable. When the flow is not aligned with the mesh (i.e., when it crosses the mesh lines obliquely), however, first-order convective discretization increases the numerical discretization error (numerical diffusion). For triangular and tetrahedral meshes, since the flow is never aligned with the mesh, you will generally

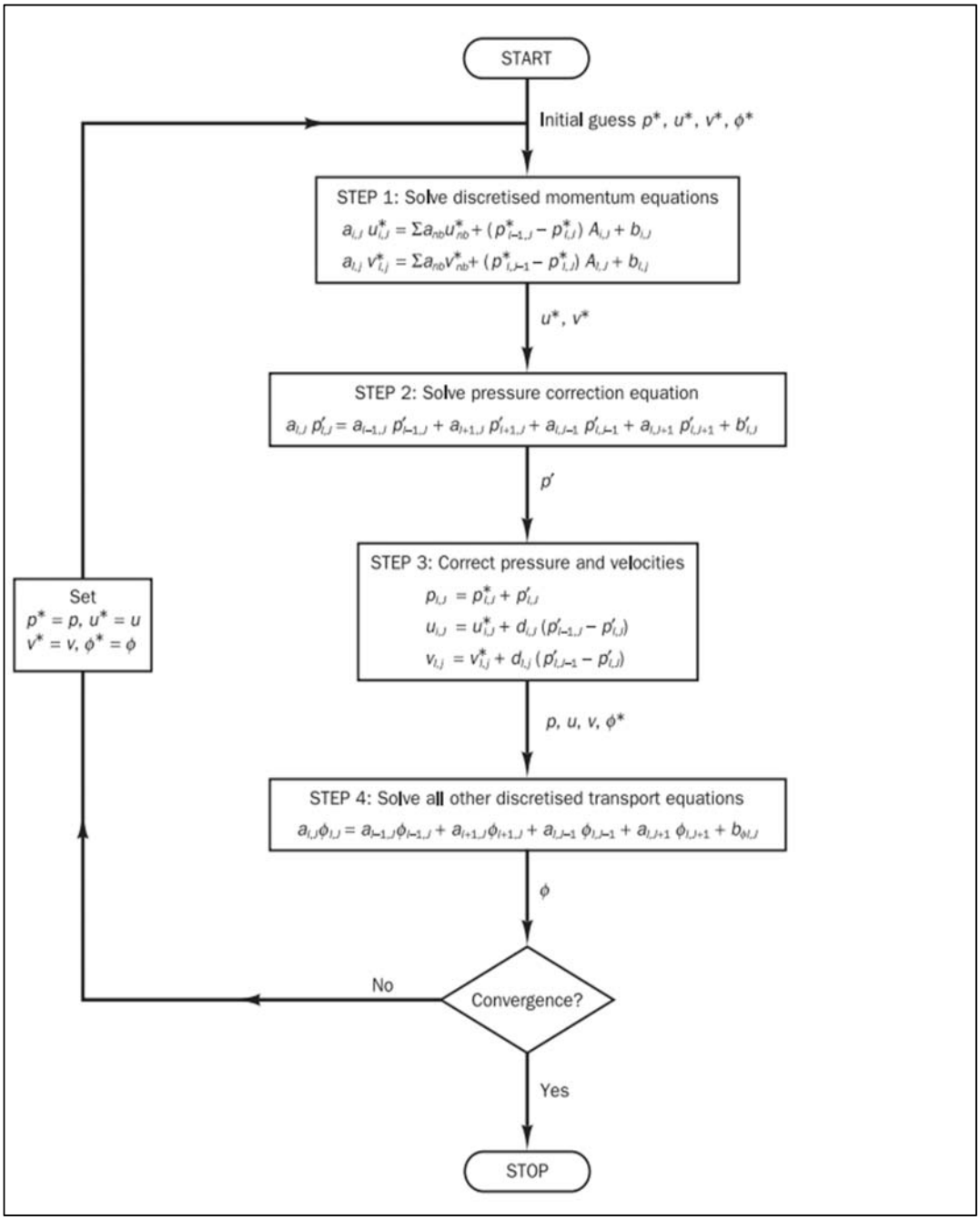

Figure 2.7 Flow process of SIMPLE algorithm

obtain more accurate results by using the second-order discretization. For quad/hex meshes, you will also obtain better results using the second-order discretization, especially for complex flows. In summary, while the first-order discretization generally yields better convergence than the second-order scheme, it generally will yield less accurate results, especially on tri/tet meshes.

For most cases, you will be able to use the second-order scheme from the start of the calculation. In some cases, however, you may need to start with the first-order scheme and then switch to the second-order scheme after a few iterations. For example, if you are running a high-Mach-number flow calculation that has an initial solution much different than the expected final solution, you will usually need to perform a few iterations with the first-order scheme and then turn on the second-order scheme and continue the calculation to convergence. Alternatively, full multigrid initialization is also available for some flow cases which allow you to proceed with the second-order scheme from the start.

For a simple flow that is aligned with the mesh (e.g., laminar flow in a rectangular duct modeled with a quadrilateral or hexahedral mesh), the numerical diffusion will be naturally low, so you can generally use the first-order scheme instead of the second-order scheme without any significant loss of accuracy.

Finally, if you run into convergence difficulties with the second-order scheme, you should try the first-order scheme instead.

In conclusion, this section has explored the fundamental concepts of CFD theory. Through the topics covered here we will be able to navigate through most of the CFD simulation software and be able to understand the models and methods which need to be used for basic fluid flow simulations.

3. Literature Review

Now we will refer to the various studies which were carried out by researchers in the field of mixing tanks and the simulations carried out on the same.

Mixing is one of the most important processes in a wide range of industries like pharmaceuticals, chemical and food. The main focus of these industries is to obtain a homogeneous mixture of two or more substances with the best mixing quality. As the mixing quality increases, the efficiency of the mixing process decreases. Thus, industries have to make a conscious decision about whether to sacrifice mixing quality or efficiency.

By the study and experiment done by John DeMoss and Kevin Cahill, it was concluded that the process of mixing is highly dependent on Reynolds number. In case of flow field being laminar the increase in mixing time will be very significant as compared to the flow being turbulent for the same tank dimensions. [14] Thus, one of the key characteristics of the mixing tank should be that the flow generated should have a high Reynolds number unless otherwise explicitly stated. Thus, it can be concluded that the mixing process is inertial dependent rather than viscous dependent.

According to the study by Tefugen Technologies Private Limited (CFD Analysis of mixing tank), it was found that this mixing efficiency is dependent on rotational speed of the impeller and the number of impeller blades. As the impeller speed increased, the process of mixing occurs rapidly throughout the tank enabling the mixing of fluids to occur quicker. However, this also increases the power consumption of the system. [18] Thus to overcome this, usually the position of impeller is manipulated. This may include changing the impeller clearance with respect to the tank bottom as well as providing an offset to the impeller. The same can be said about the parameter of number of impeller blades.

The same study also points that the efficiency is also a function of viscosity of the fluid materials which are to be mixed. Highly viscous fluids will require more power to displace to initiate the process of mixing. . [18] One of the methods to overcome this problem is to change the temperature of operation so that the viscosity of the fluids lessens. However, this is not always possible as in cases of critical chemicals and fluids, a chemical reaction may occur which will cause wastage as well as may cause damage and is also more cost intensive. Thus, a better method to overcome this problem is to change the type of impeller used. Depending upon the viscosity of the fluids, there are different impellers which can be used for mixing process.

By D. Ankamma Rao and P. Sivashanmugam, it was concluded that the impellers which have been modified by means of cuts in blades produce better results than standard impellers. This result as they impart more shearing effect to the fluid and consume less power as compared to standard impellers. This also points to the characteristics that impellers having unique designs like anchor blade, ribbon blade and others are beneficial to be used for highly viscous fluids as they produce high shearing effects. [15] Thus it can be concluded that for highly viscous fluids high shearing impeller blades are required.

The study by A. Delafosse, J. Morchaina, P. Guiraud, A. Liné finds that the Large Eddy Simulation (LES) is more accurate than Reynolds Average Navier Stokes (RANS) method. [13] However, LES approach is out of reach in most practical settings due to the rather intense computations required.

Similarly, by A. Delafosse, J. Morchain, P. Guiraud and A. Liné by it was concluded the RANS turbulence models like k–e, SST, SST–CC, SAS–SST and SSG–RSM predict the mean axial and tangential velocities reasonably well, but they tend to under-predict the decay of mean radial velocity away from the impeller. [13] Thus, the most basic and robust k-ε should be used.

The paper by Harshal Patil and group explores the idea of using Multiple Reference Frame (MRF) approach for CFD simulations. Here multiple parameters like power number, pumping number and turbulent energy dissipation rate were validated and found to be having deviation with acceptable limits from the true values. As this approach is less computationally intensive than sliding mesh approach, it was chosen for CFD simulations. [17] Also, the optimum dimensions and position of the inner domain of the MRF approach with respect to the outer domain were found out.

The research done by Dragan D. Nikolić in the paper presents the experimental data about Radial, Propeller and Inclined impellers. The mixing time of each impeller was found at 300, 400, 500 and 700 rpms in both the unbaffled and baffled configurations of the mixing tank at 95% and 99% mixing quality. The mixing time was found out by using Laser Induced Fluorescence (LIF) technique. [12] This data was then used as validation and cross checked against CFD simulation.

By studying and understanding the different research conducted on mixing tank, we can identify and fix the parameters which are to be used for designing the mixing tank and for the simulation which is to be carried out for estimation of mixing time computationally.

4. Methodology

After understanding the methods and techniques which are to be used for simulation, we will now understand the simulation process from geometry designing, mesh generation, setting boundary conditions, solver settings, stopping criteria and results.

4.1. Geometry model

A 3D model has been created to represent the geometry of the tank, which can be viewed in the figure 4.1. The tank has an approximate volume of $1x10^6 mm^3$. The analysis is done on three types of impellers namely radial, axial, and propeller. The radial impeller has four number of blades whereas Propeller and Inclined impeller has three blades that direct the flow of fluid in mixing tank. There is no angular orientation for Radial blades, So the radial blades are placed 90 degrees. While Inclined and Propeller are placed at 45-degree angle. All blades cover the entire space around the shaft equally. Additionally, the radial blades are straight down, while the axial and propeller blades are tilted downwards to enhance the mixing capabilities of the shaft. The model, including the shaft and the tank, is depicted in the figure 4.1. The impeller diameter is 38mm, and it is located 42.52mm from the bottom of the tank. The most relevant measurements are summarized in the figure 4.1.

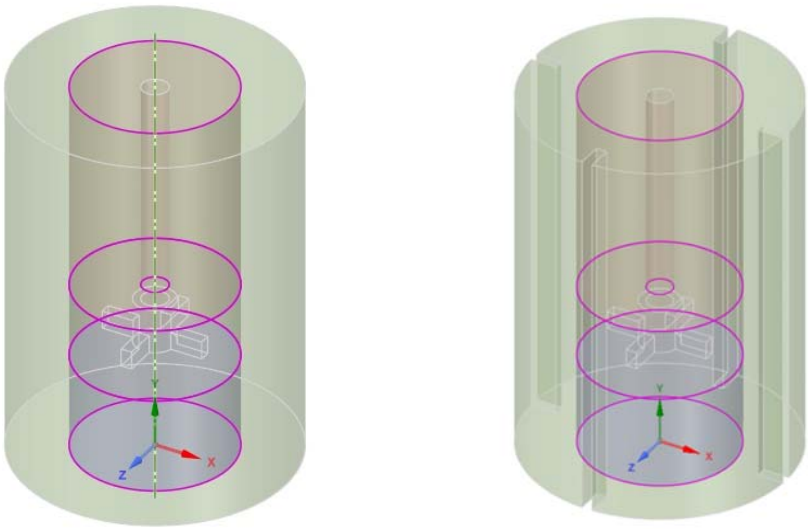

Figure 4.1: Model used with the interface separating the two designated regions for unbaffled and baffled configuration.

As stated in the context of model rotations, it is essential to define two distinct regions. An inner domain is generated near the cones, enclosing them and their closest proximity. On the other hand, the outer domain is the remaining fluid volume, which is separated from the inner domain using an interface.

Table 4.1 Measures of the tank

Parameter	Value	Units
Diameter Tank	50	mm
Height Tank	127.32	mm
Diameter Impeller	38.1	mm

As mentioned above, three types of impellers have been used, namely.

- Radial blade (Figure 4.2)
- Inclined blade (Figure 4.4)
- Propeller blade (Figure 4.3)

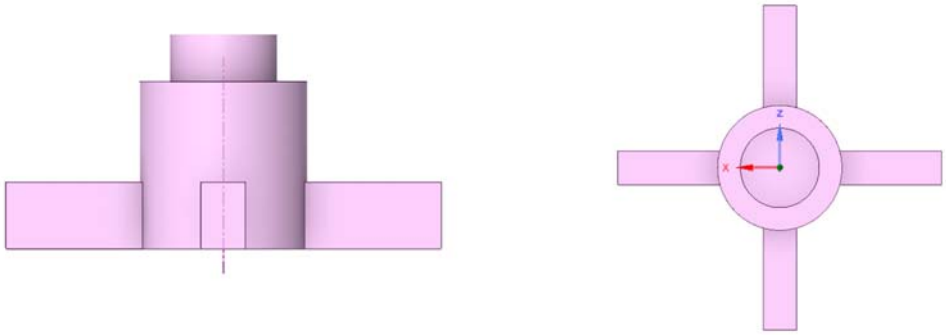

Figure 4.2: Radial impeller detailed geometry

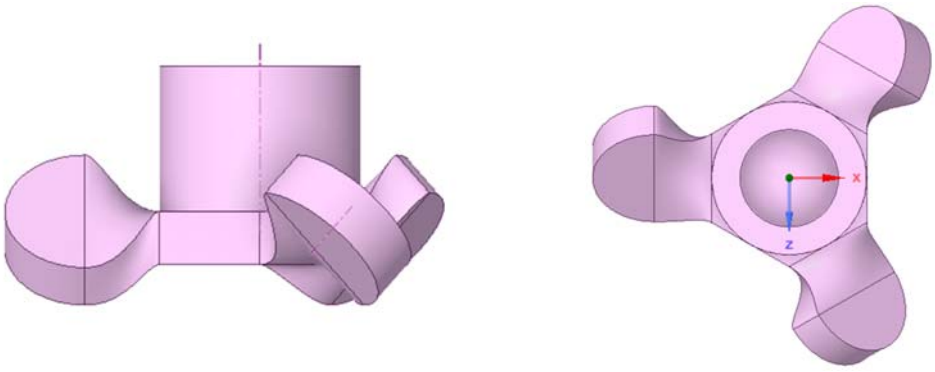

Figure 4.3: Propeller impeller detailed geometry

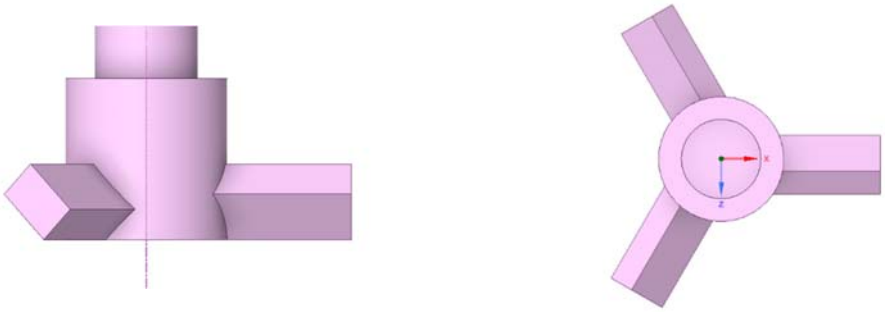

Figure 4.4: Inclined impeller detailed geometry

4.2. Mesh

To solve the Partial Differential Equations seen in governing equations, the model is discretized in time and space. In this section the mesh that subdivides the domain in elements is analysed.

Figure 4.5 Mesh generated.

For the tank equipped with the radial impeller, a mesh sensitivity is performed. With it, the independence of the results with the mesh is under inspection. Two different meshes are studied. Tetrahedral mesh, is used in the inner domain and the hexagonal mesh is used in the outer domain resolve correctly the flow

close to walls. Most of the refinements and controls are relative to this value and thus, by changing this base size, the mesh is parametrically affected. However, to increase the accuracy of the overall iteration performance, different refinements are included in the meshing process. Every important surface is refined according to its requisites. The impeller and the shaft, due to its production of turbulence, are refined to have a smaller targeted surface size. Having then, every refinement and default control scaled with the base size, the abovementioned four meshes vary precisely that parameter. Optimizing the mesh is one of the key steps when modelling due to its significant benefits in timesaving and error avoiding.

4.3. Boundary conditions

To accurately model the fluid flow, it is necessary to define two distinct domains: an inner (rotating) domain and an outer (Stationary) domain. The inner (rotating) domain needs to define how the fluid interacts with impeller walls. Since it is solid materials, the fluid cannot go through and therefore should be defined as wall. Furthermore, the fluid in direct contact with the wall act according to the adhesion law, which basically makes these fluid travel attached to the wall. For considering this effect, the *No-Slip* condition is activated. To compute the rotation, the procedure is different depending on the approach used as one can see in table 4.2**.** When MRF is used, a Rotational Reference Frame must be applied to the whole region. Since the impeller speed is predefined as 300,400,500,700 rpm clockwise according to the shaft axis. Since to activate this rotation is applied to the whole interdomain. Outer domain contains the free surface and the rest of walls not included in the inner domain. For the walls, the same principle is applied, so these as a shaft and *Wall, No-Slip*. In the free surface, interactions with air exist. This nothing but a rough simplification of reality that allows certain movement of the phases sliding with the false top wall**.**

The shaft is given the moving wall condition for the rotation. The stationary region contains the free surface, and the rest tank wall are not included in the inner domain. For the impeller walls, the same principle is applied, so these are defined as Wall, No-Slip. In the free surface, interactions with air exist. To correctly model this behaviour, VOF should be used. To reduce the computational complexity of this boundary, the constraint is chosen to be as *Wall, Slip*. This nothing but a rough simplification of reality that allows certain movement of the phases sliding with the false top wall. Since the air viscosity is low, it is more correct to model the wall with the zero-shear condition than with the *No-Slip* one. These walls, have the *Wall, No-Slip* condition, but moreover, as previously mentioned these impeller walls should spin at 300, 400, 500, 700 rpm clockwise. Since no motion is assigned to the general domain, a wall relative rotation is assigned to it, of exactly the mentioned rotation rate. Finally, the interface is present

as the layer that connects both domains and oversees transferring quantities between the two entities. A summary of all the boundary conditions applied can be seen in table 4.2.

Table 4.2 Boundary conditions of the model.

Region Boundary	Boundary Condition
Spinning	**MRF: Moving Reference Frame (300, 400, 500 and 700 rpm respectively)**
Agitator Wall	No Slip
Stationary	**Lab reference frame (stationary)**
Shaft	Wall. No Slip. Wall relative rotation (300, 400, 500 and 700 rpm respectively)

4.4. Solver settings

The continua are created using the models shown in table 4.3. With them, the general physics that rule the behaviour of the system, are defined. Two different turbulence models were performed for this tank analysis. a model sensitivity is performed with the aim to evaluate the different predictions that these could offer and therefore the robustness of the results with the choice of model. The chosen models were the Realizable $k-\varepsilon$ and SST $k-\omega$ both. The Realizable $k-\varepsilon$ was selected because it used less computational complexity. As flow solvers, MRF is solved with SIMPLE Flow to get an initial solution of the fields. In general, SIMPLE solver shown more stability when running MRF, which allowed a smoother convergence of residuals, thanks to solving the equations. Regarding the timestep for unsteady simulations, it is chosen as $\Delta t = 0.0005$s, when using RANS turbulent models. This value is obtained based on the frequencies that wanted to be resolved. Since the highest frequencies were not interesting for the project, the timestep is set based entirely on the rotation rate of the stirrer and the desired sampling to resolve these frequencies correctly.

Table 4.3: General models for the physics setup.

Physics	Model	
Continua	Space	Three-dimensional
	Phase	Liquid
	Regime	Turbulent
	Density	Constant density
Turbulence models		k-epsilon
Flow solver		SIMPLE
Time Solver		Steady
Optional Models		Gravity

4.5. Stopping criteria

Table 4.4: Stopping criteria set for the simulations

Monitor	Type	Value
Continuity	Minimum	1×10^{-5}
X-velocity	Minimum	1×10^{-5}
Y-velocity	Minimum	1×10^{-5}
Z-velocity	Minimum	1×10^{-5}
K	Minimum	1×10^{-5}
Epsilon	Minimum	1×10^{-5}
Tracer	Minimum	1×10^{-5}
Maximum iterations (unsteady cases)	-	35

The stopping criteria are used to control the behaviour of the simulation. They monitor the residuals and various engineering parameters, such as torque, velocity, and convergence, to determine whether the solution is correct. The criteria are set to ensure convergence, with specific values provided in table 4.3. Residuals such as continuity error, x-velocity, y-velocity, z-velocity, k, epsilon, and Tracer are monitored, and the criteria may be more flexible for unsteady cases, leading to a slight increase in the values set in the table. In addition to residuals, engineering variables such as torque and velocity must

also be monitored to ensure they are at an acceptable error level. The criteria specified in table 4.3 are used to force these parameters to converge within each time-step. Apart from the residuals, some engineering variables must be monitored, to reassure that the parameters of interest are also at a correct error level. In this case, the engineering variable to monitor is the velocity.

4.6. Post-processing

Along with the domain, different probes are situated to post-process information during the simulation run, and after its ending. These probes must be located strategically, to capture the desired effects and behaviour correctly and not miss important information. The tank equipped with the impeller. The unbaffled tank configuration is symmetric but the baffled tank configuration is not symmetric. Due to these special conditions, the total amount of probes is reduced to a few sections and planes, being able to understand from them the behaviour of the whole domain. In figure 4.5 different lines and points used for monitoring variables are represented. As can be observed, both the lines and the points are located in the cross-section plane and discretizing the domain height. With these divisions, the flow fields of interest can be tracked.

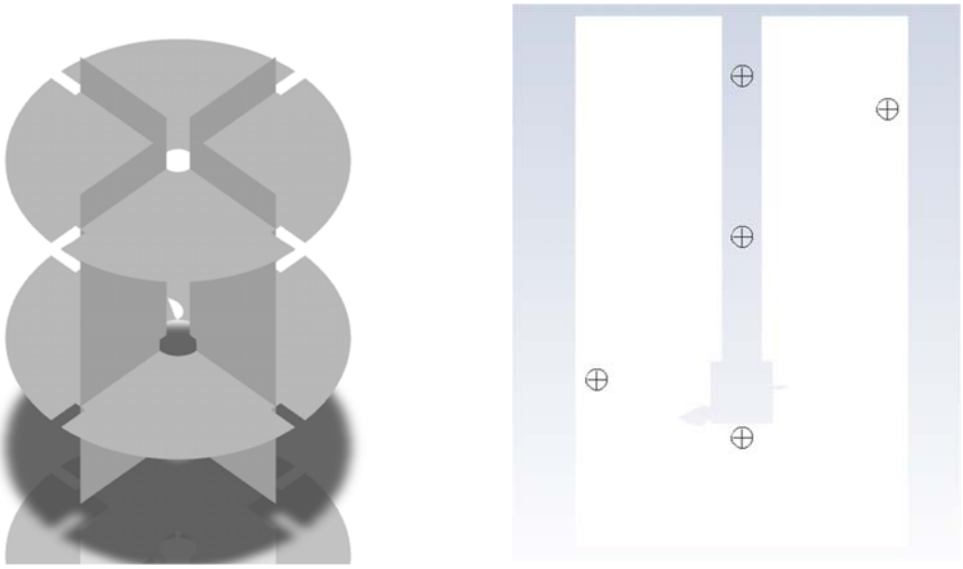

Figure 4.6: Probes for Post processing

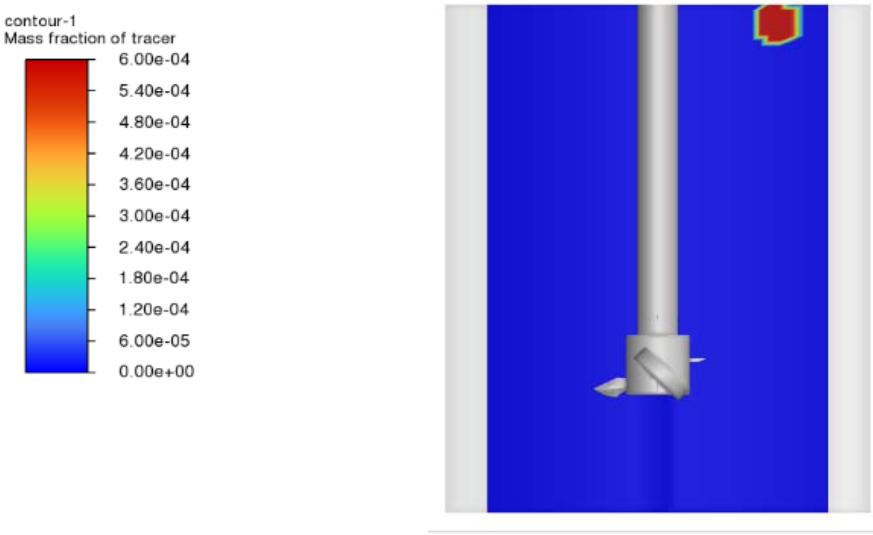

Figure 4.7: Tracer region

Now we will understand the different results obtained and interpret them so that they can be validated against the experimental time found out by the paper.

5. Result and Discussion

5.1. Flow Fields

In this section, the flow field simulations are showed. By flow field simulations, it is implied that no tracer is included in this analysis. These set of cases aim to determine how the stirrer acts, possible lifting capabilities and evaluating the quality of the methodology used.

5.2. Setting up velocity

The velocity developed and simulated by different models would significantly affect mixing time value. To verify the accuracy of the model used, we simulated Dragan's vessel and compared with their experiments. [12] the simulations agree well with experimental results. There is large discrepancy with experimental data in the impeller zone, which may be because the k – ϵ model used in our work is established based on isotropic turbulent flow. The k – ϵ model cannot correctly describe the strongly anisotropic flow in the impeller zone. However, there is still no proper model to describe accurately the complex single-phase flow in the impeller zone. The residual plot used for convergence is shown in figure 5.1.

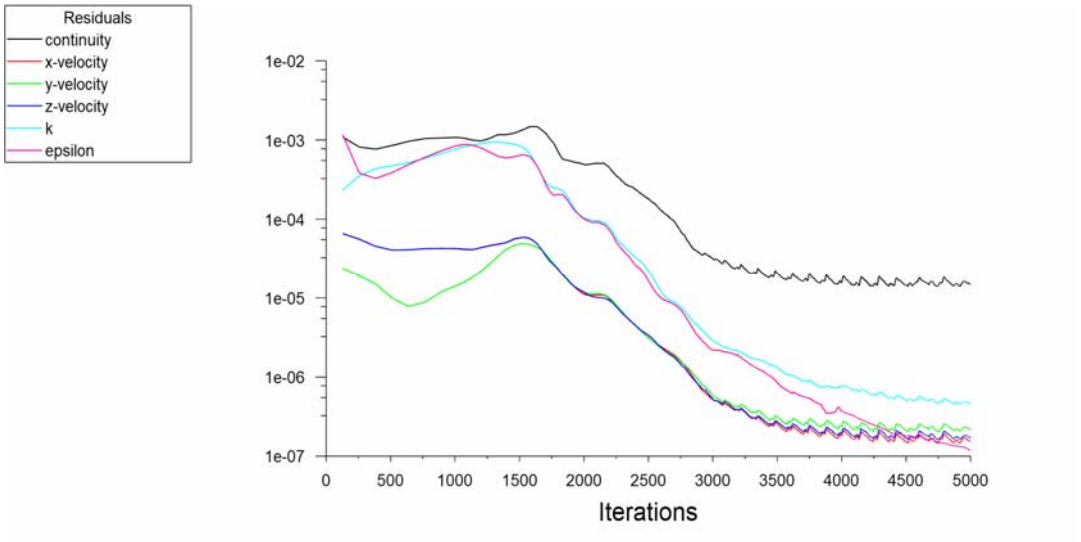

Figure 5.1: Convergence

5.3. Mixing Time

The mixing times were obtained for impeller agitation speeds of 300,400,500 and 700 rpm, at clearance level of (T/3) for all the studied impellers. This can be seen in the figures.

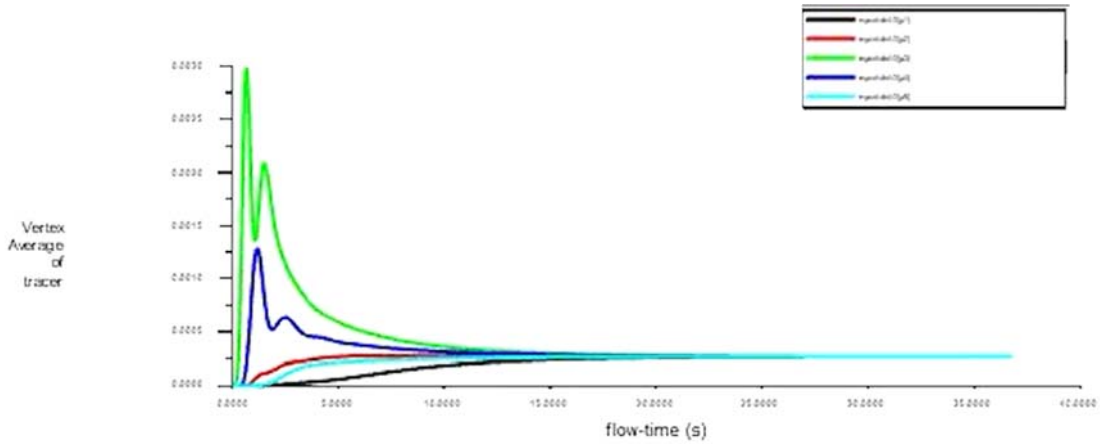

Figure 5.3: Radial Impeller Baffled @ 300 RPM

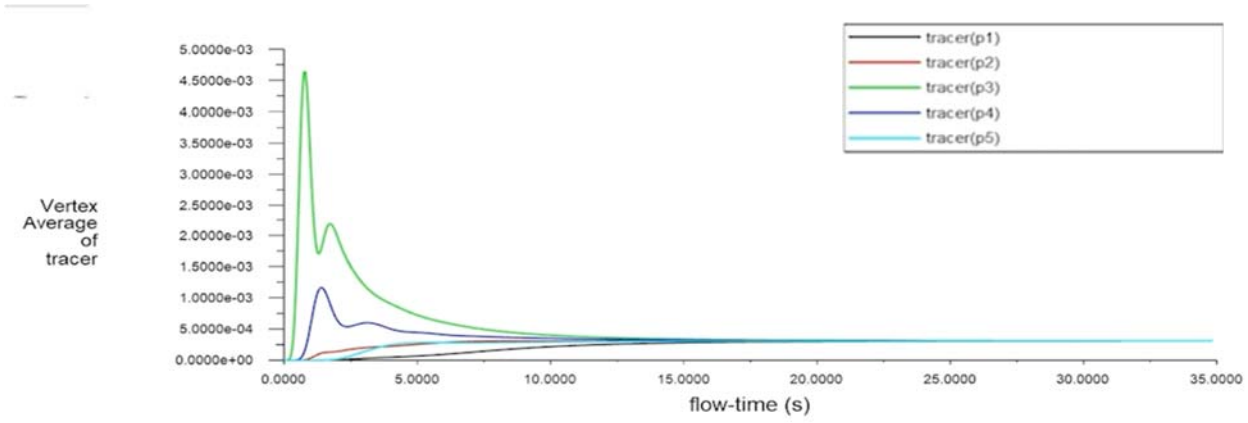

Figure 5.4: Radial Impeller Unbaffled @ 300 RPM

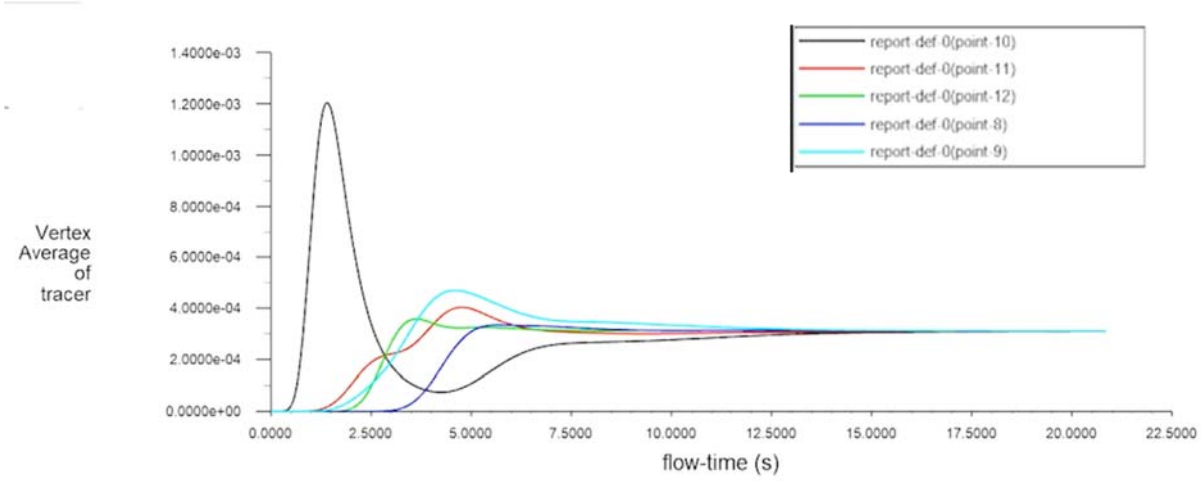

Figure 5.5: Inclined Impeller Baffled @ 300 RPM

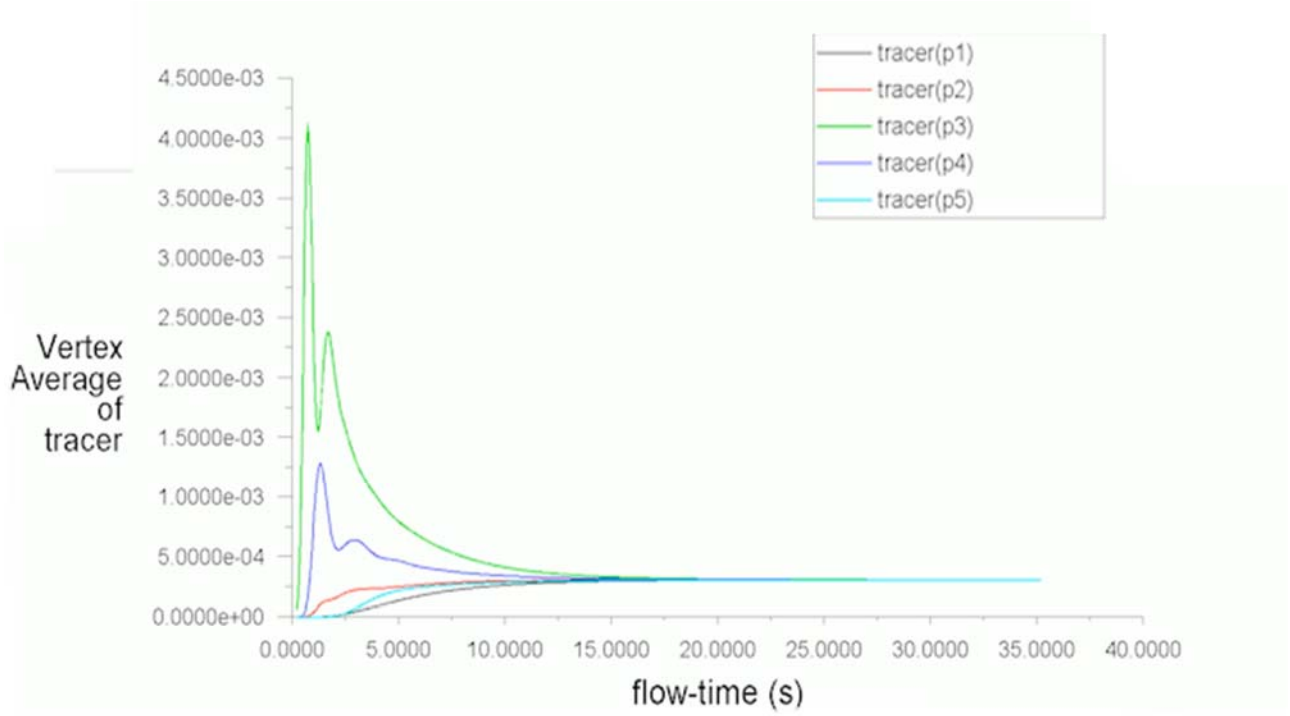

Figure 5.6: Inclined Impeller Unbaffled @ 300 RPM

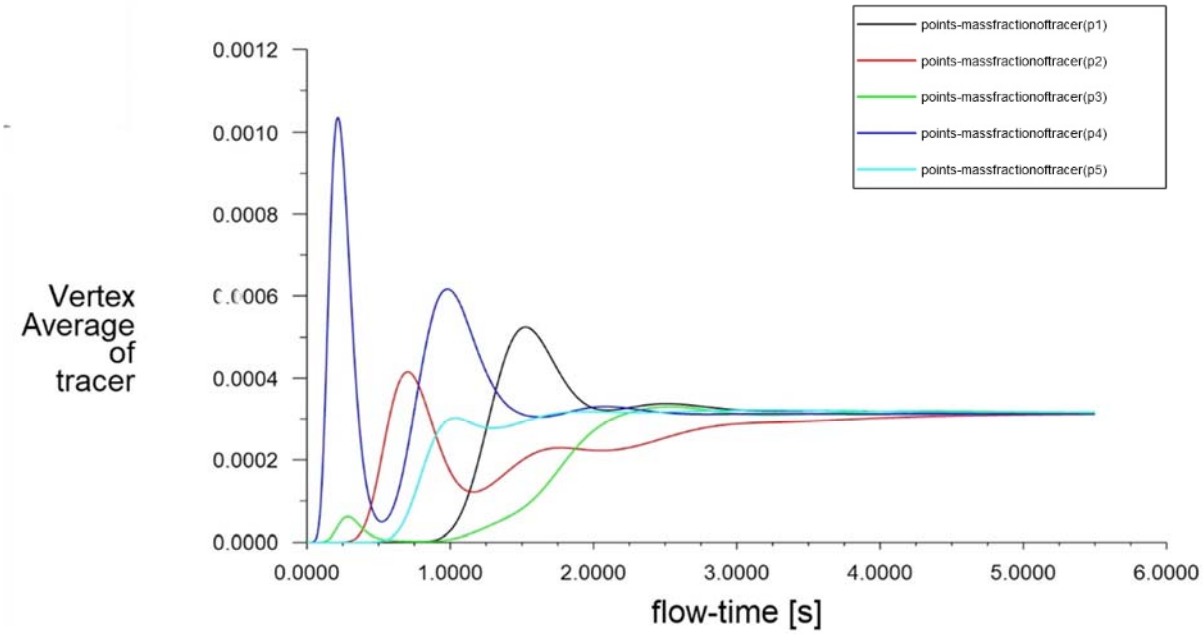

Figure 5.7: Propeller Impeller Baffled @ 300 RPM

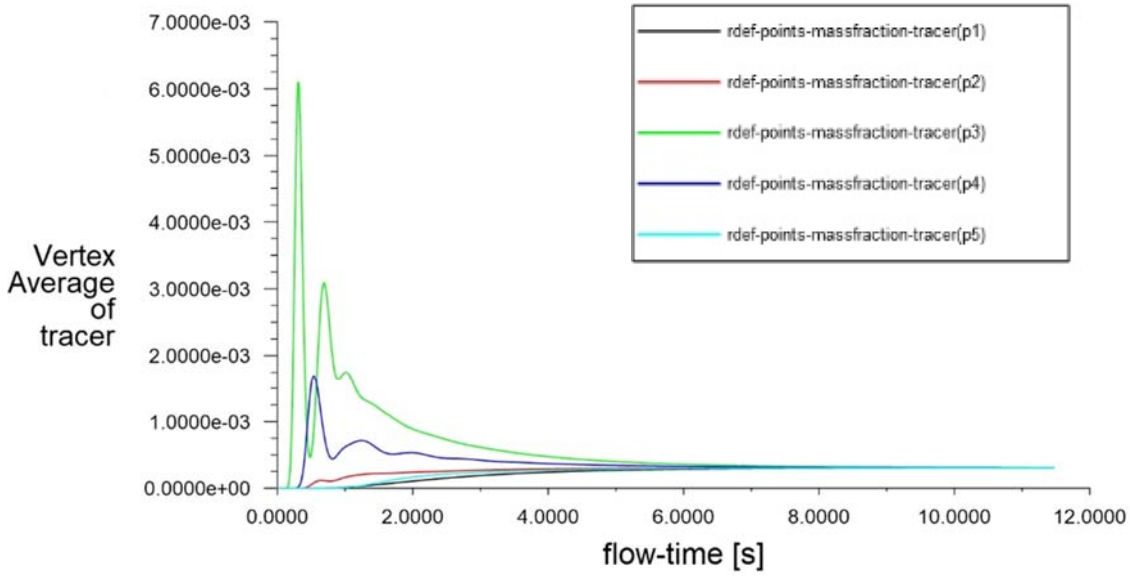

Figure 5.8: Propeller Impeller Unbaffled @ 300 RPM

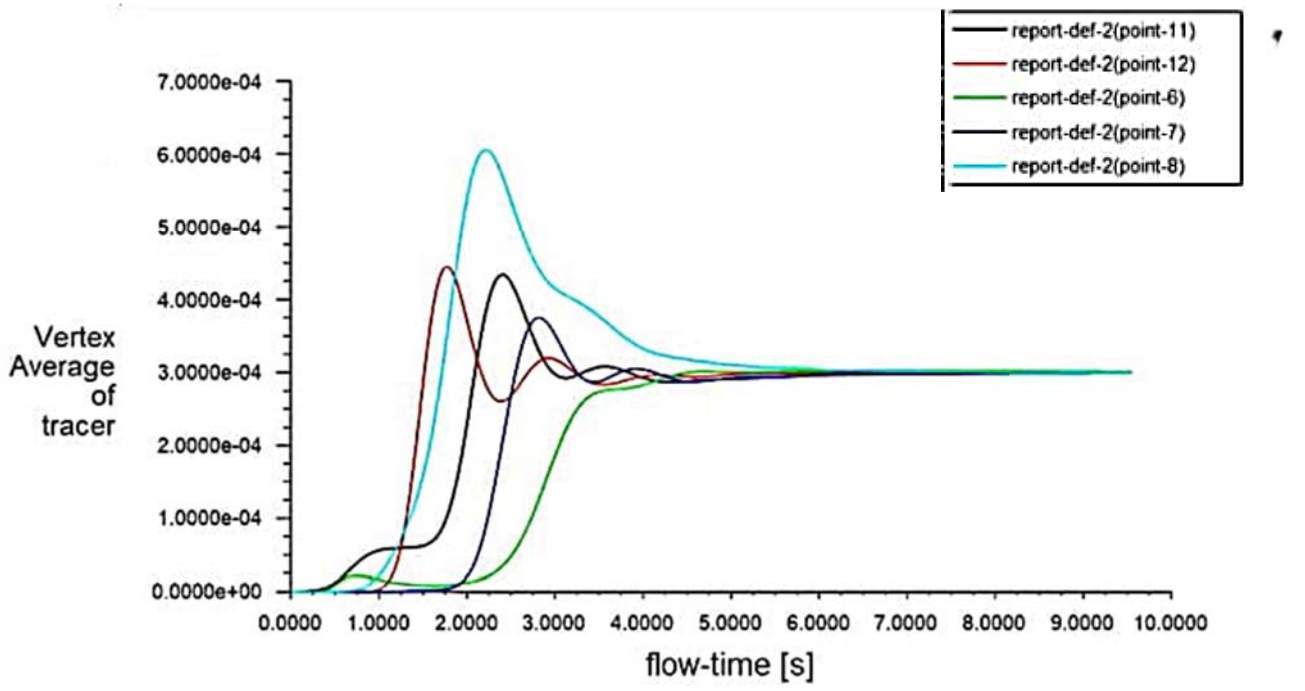

Figure 5.9: Radial Impeller Baffled @ 400 RPM

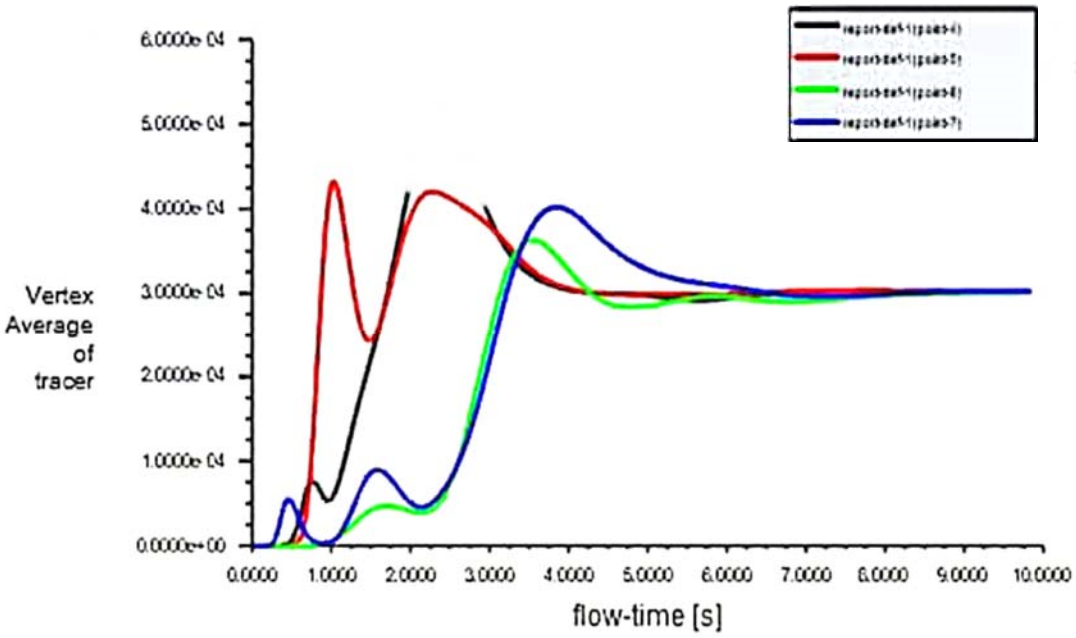

Figure 5.10: Radial Impeller Unbaffled @ 400 RPM

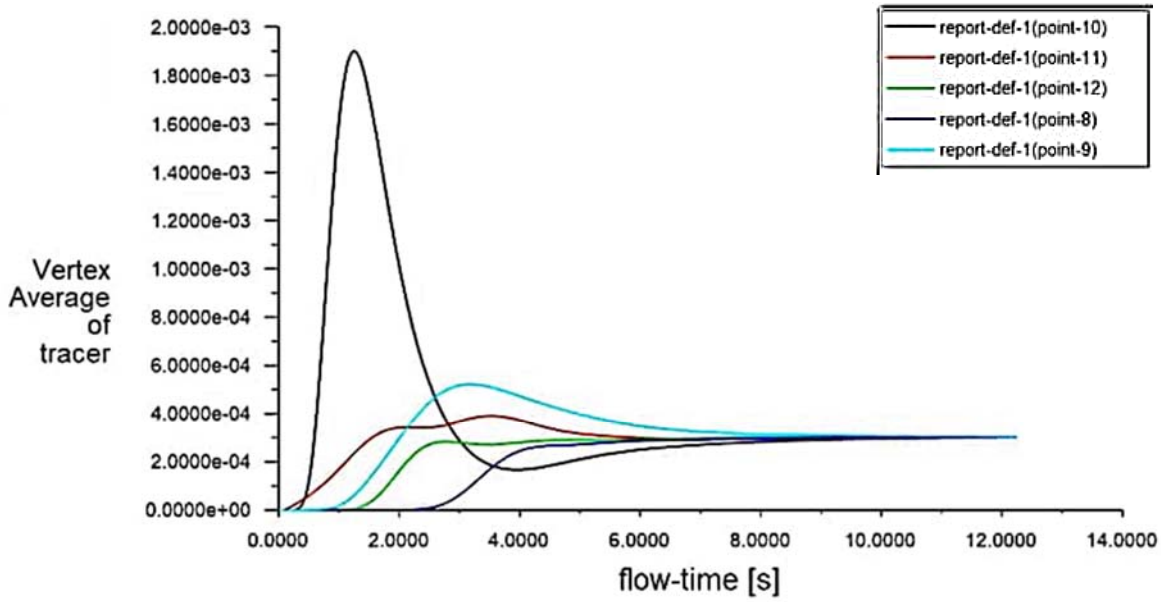

Figure 5.11: Inclined Impeller Baffled @ 400 RPM

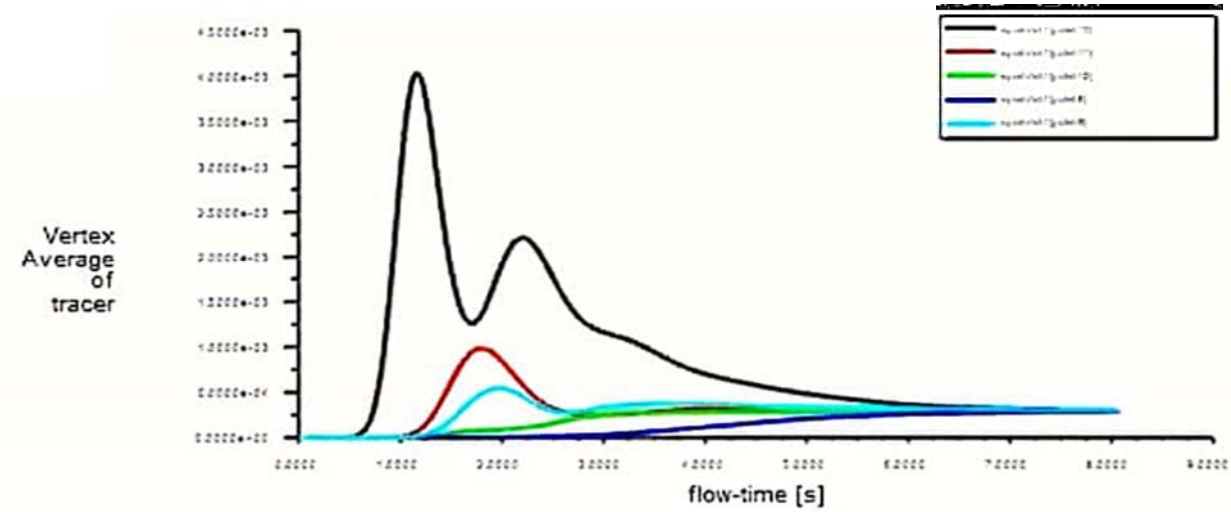

Figure 5.12: Inclined Impeller Unbaffled @ 400 RPM

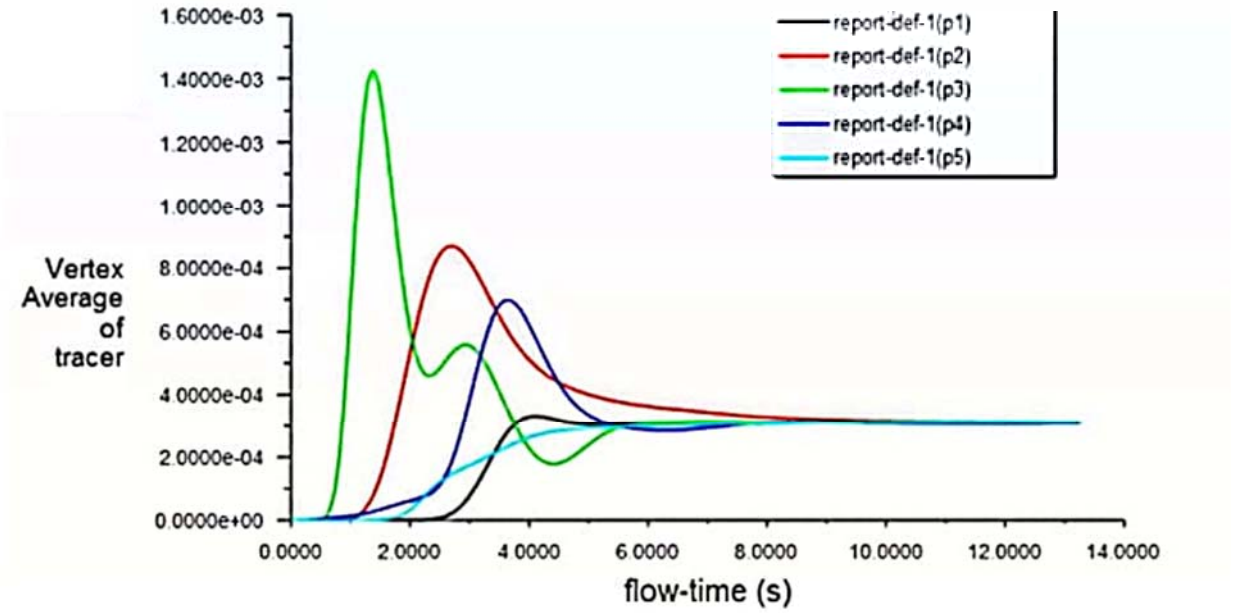

Figure 5.13: Propeller Impeller Baffled @ 400 RPM

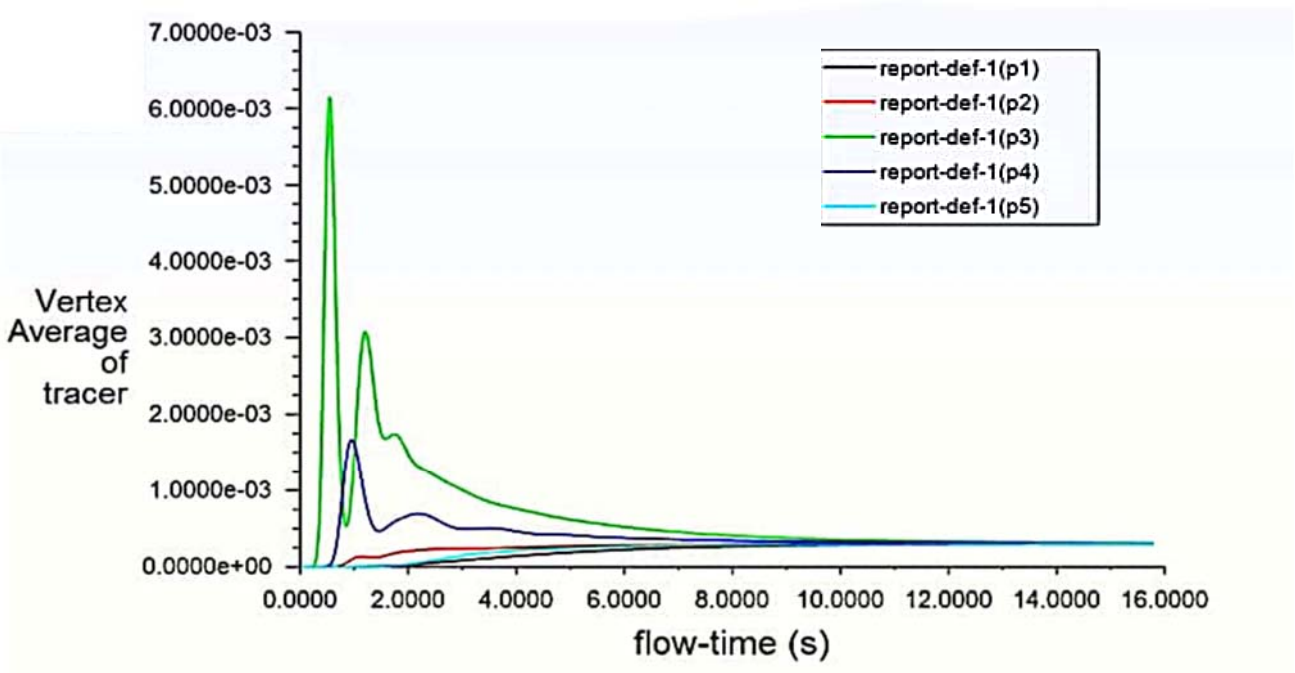

Figure 5.14: Propeller impeller Unbaffled @ 400 RPM

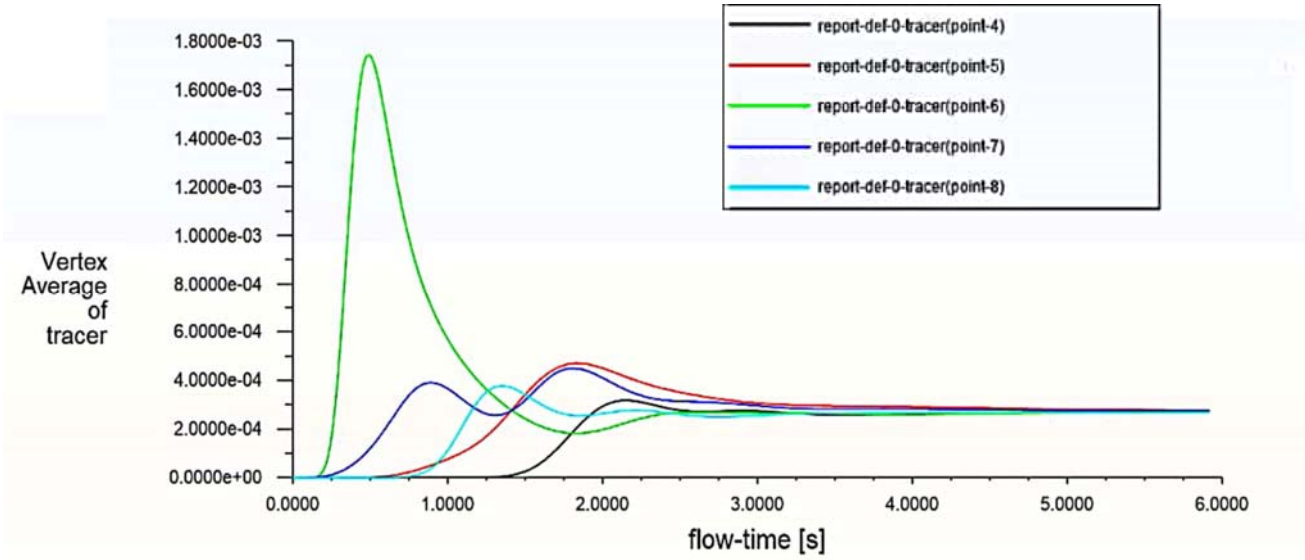

Figure 5.15: Radial Impeller Baffled @ 500 RPM

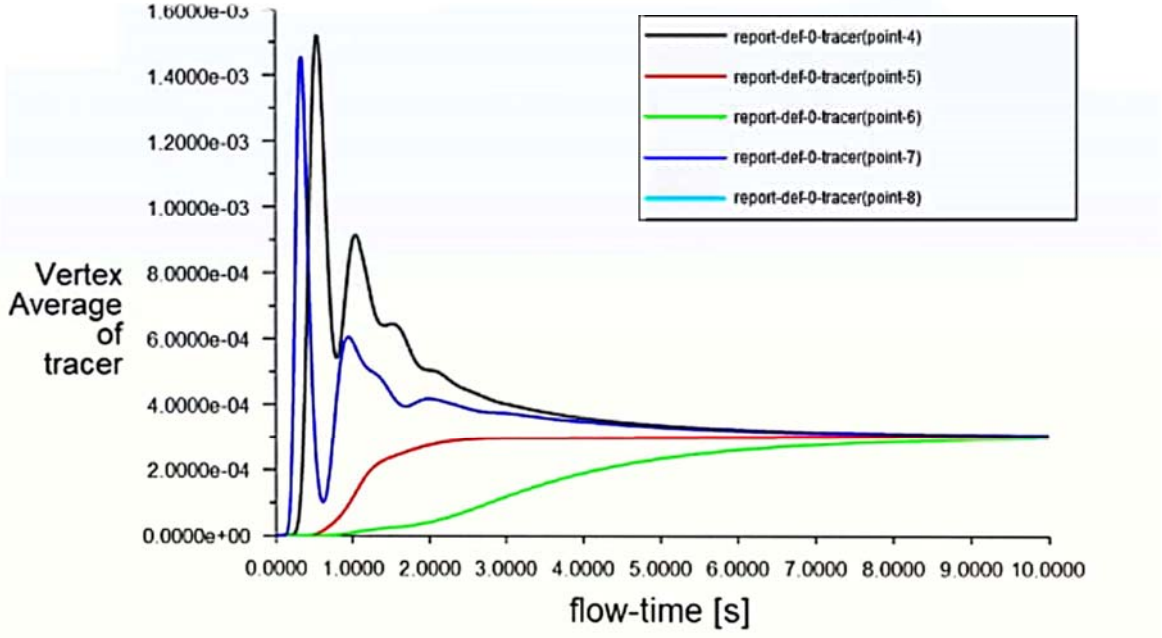

Figure 5.16: Radial Impeller Unbaffled @ 500 RPM

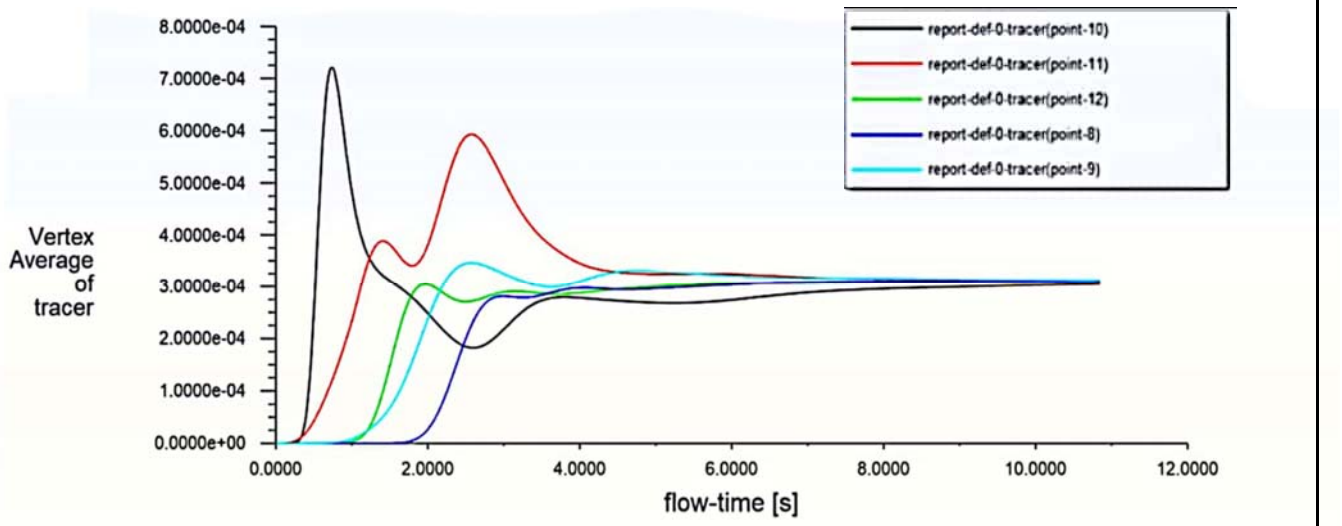

Figure 5.17: Inclined Impeller Baffled @ 500 RPM

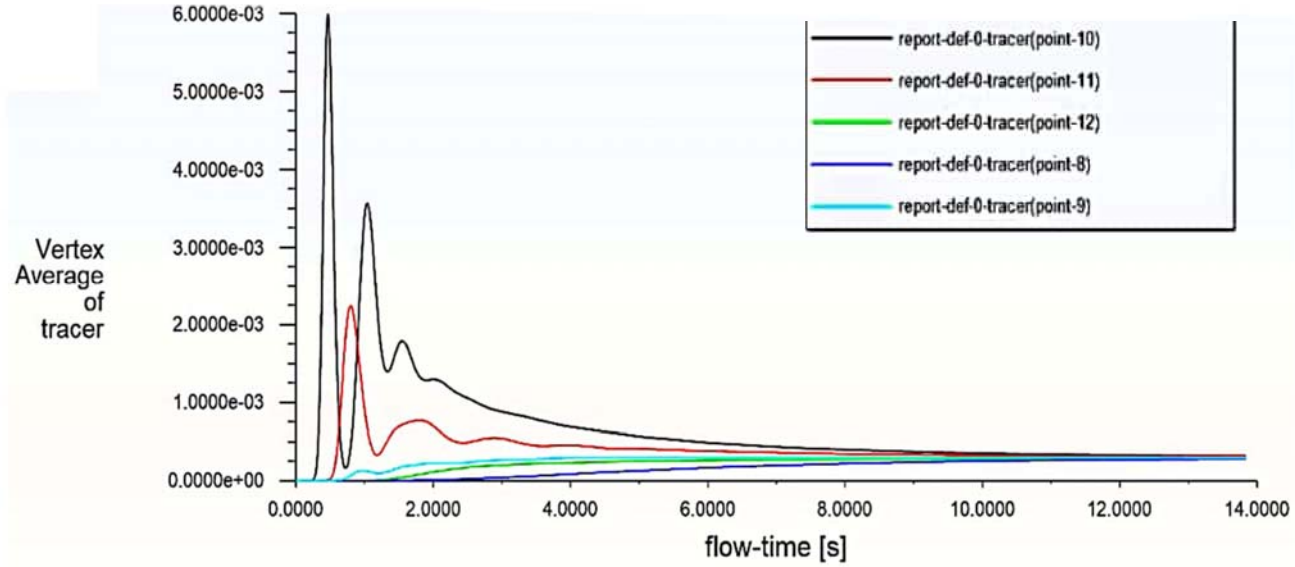

Figure 5.18: Inclined Impeller Unbaffled @ 500 RPM

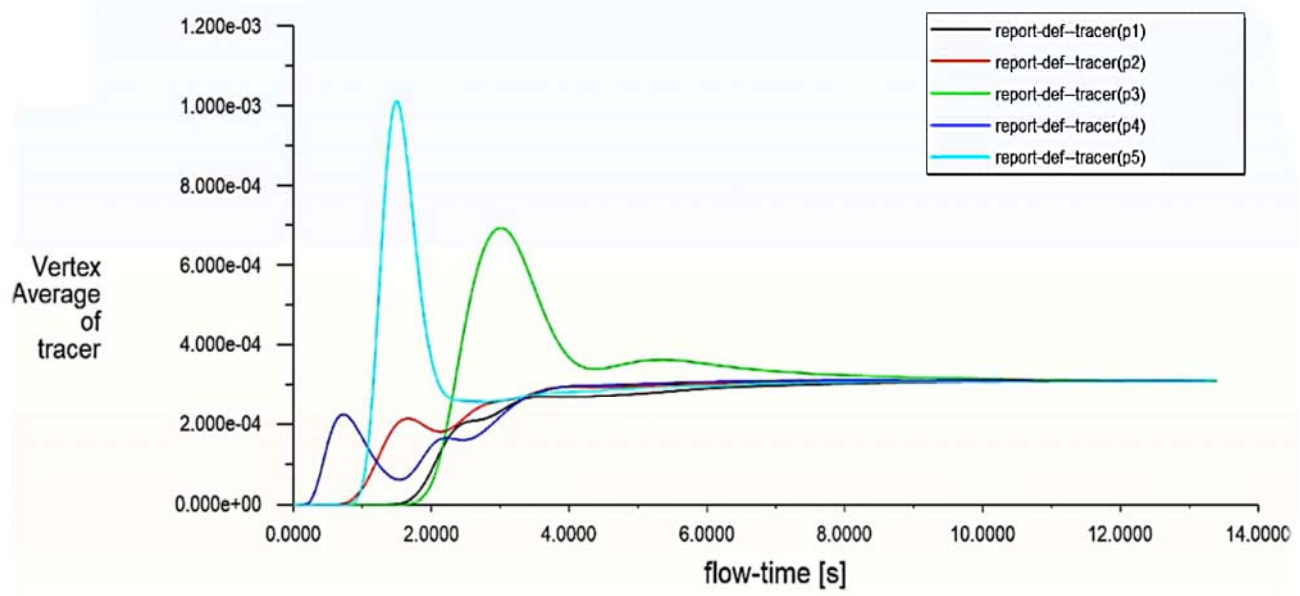

Figure 5.19: Propeller Impeller Baffled @ 500 RPM

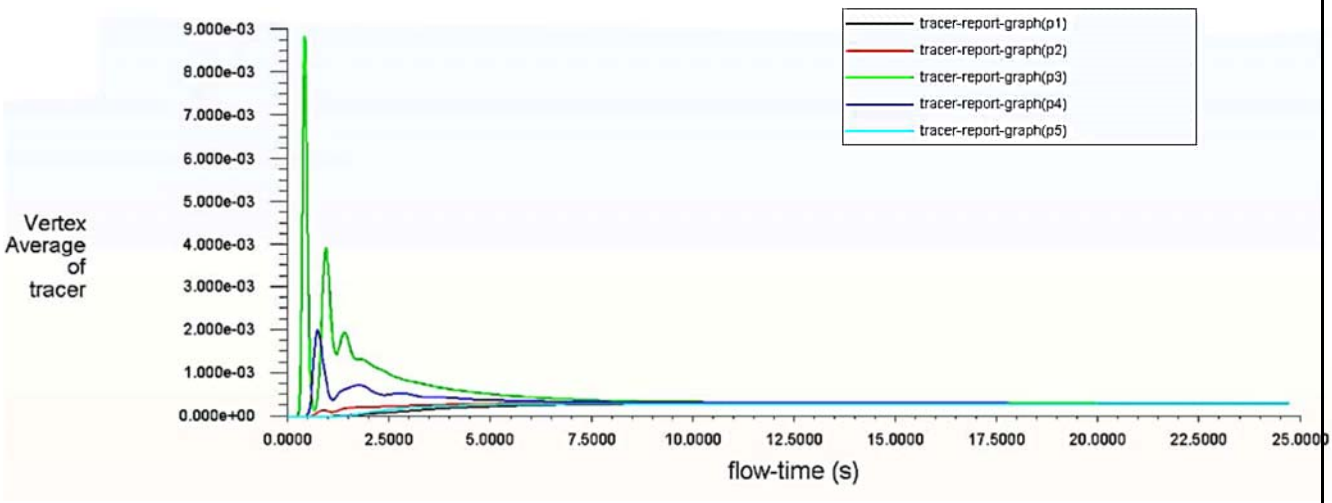

Figure 5.20: Propeller Impeller Unbaffled @ 500 RPM

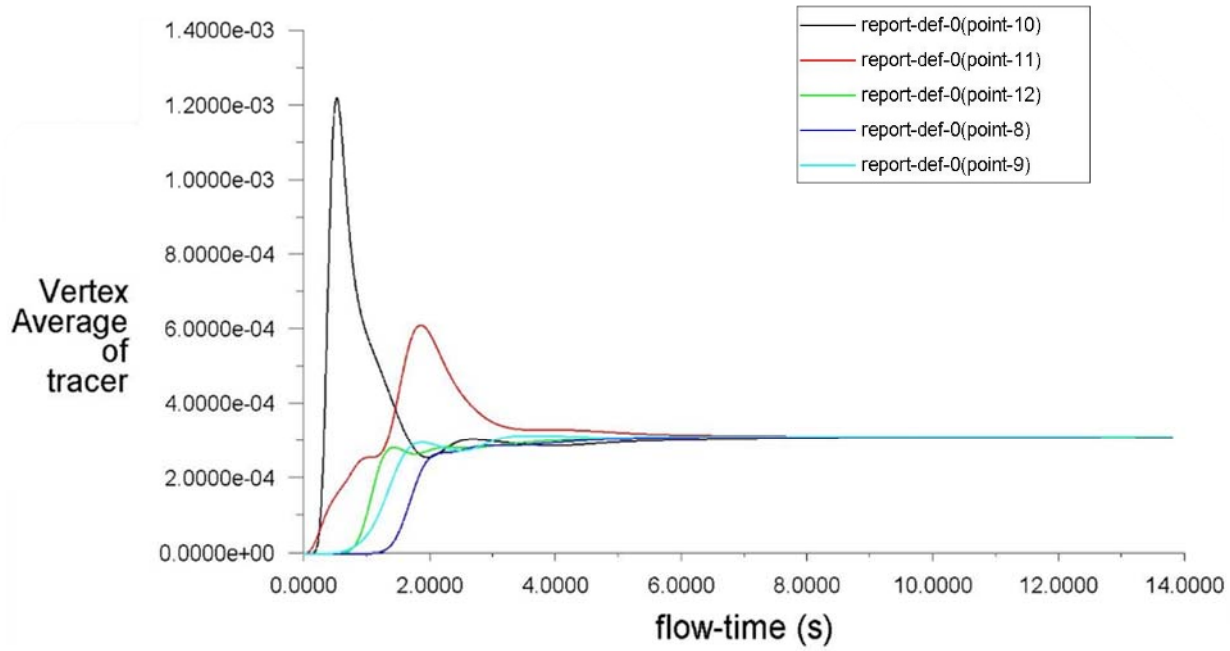

Figure 5.21: Radial Impeller Baffled @ 700 RPM

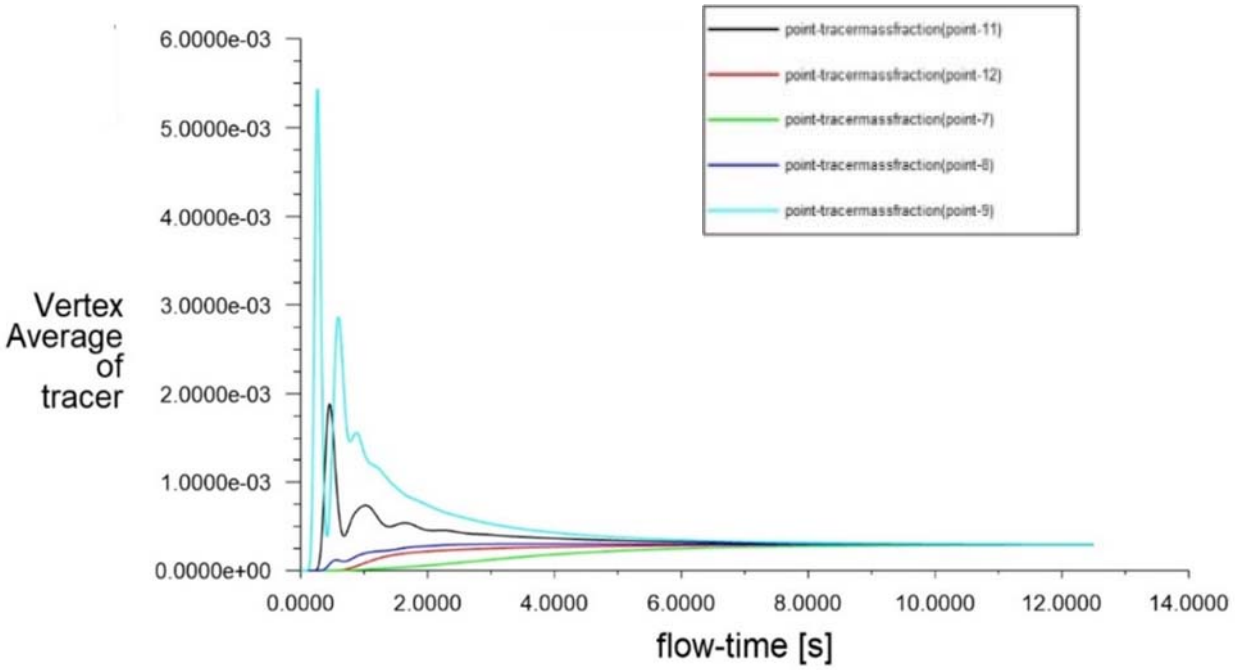

Figure 5.22: Radial Impeller Unbaffled @ 700 RPM

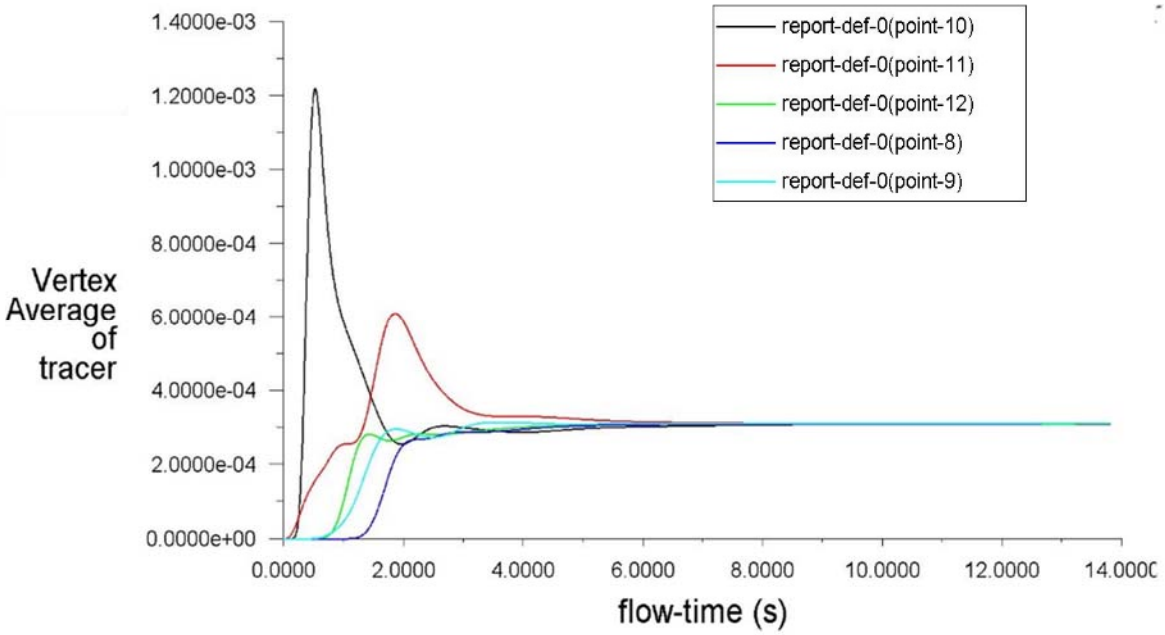

Figure 5.23: Inclined Impeller Baffled @ 700 RPM

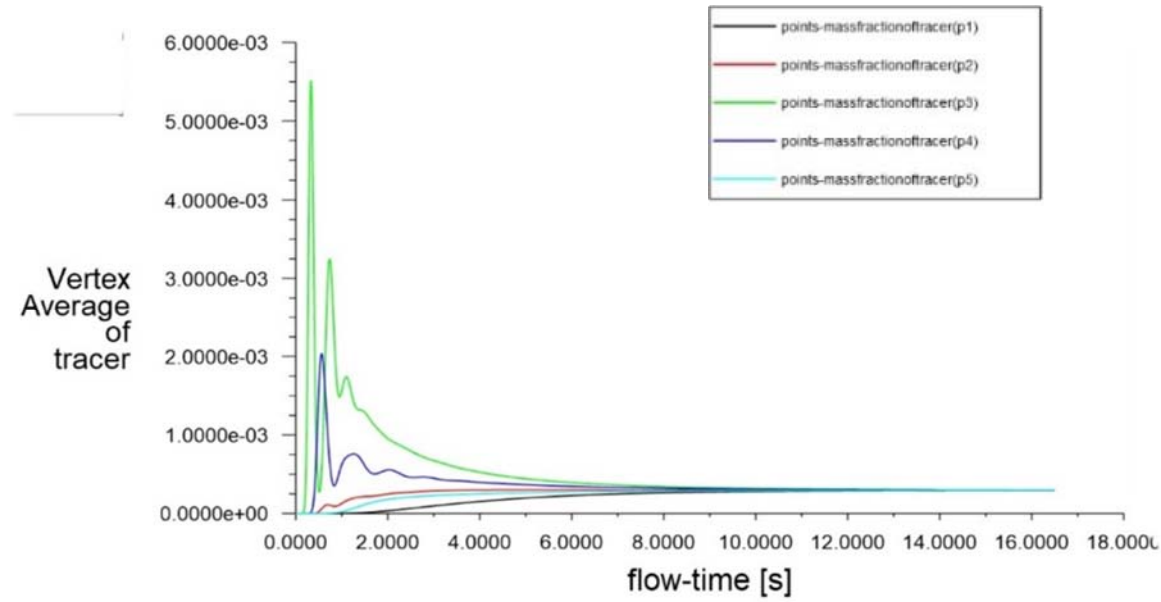

Figure 5.24: Inclined Impeller Unbaffled @ 700 RPM

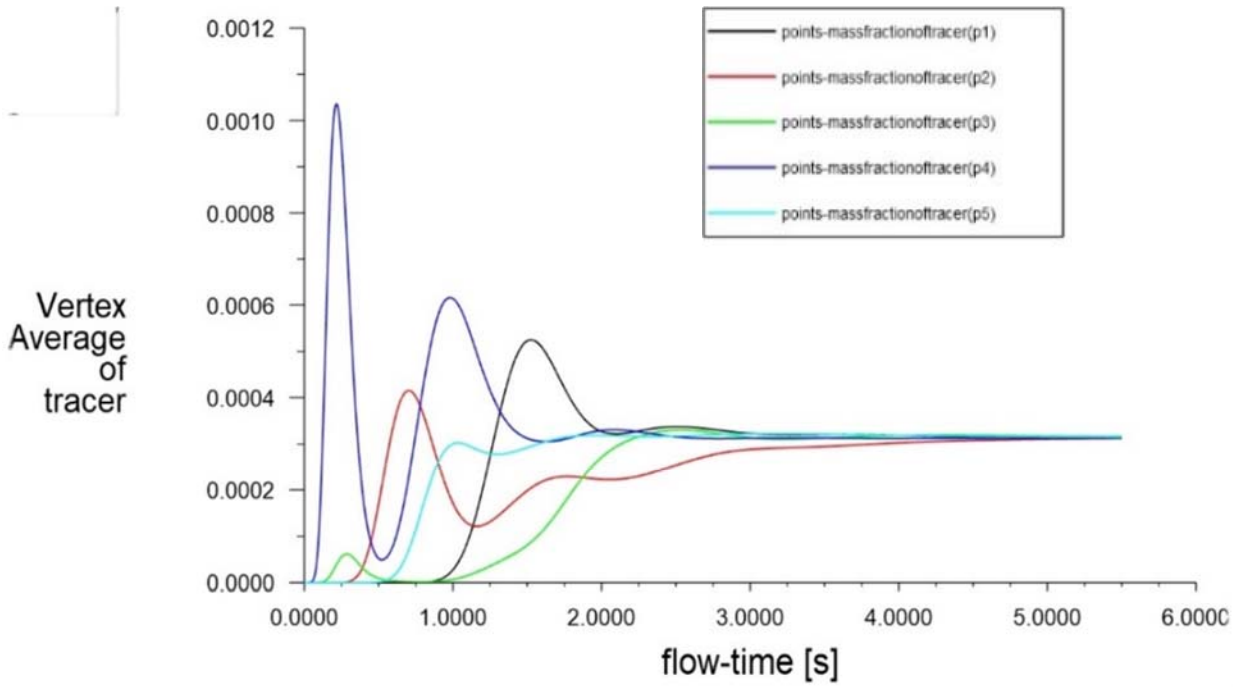

Figure 5.25: Propeller Impeller Baffled @ 700 RPM

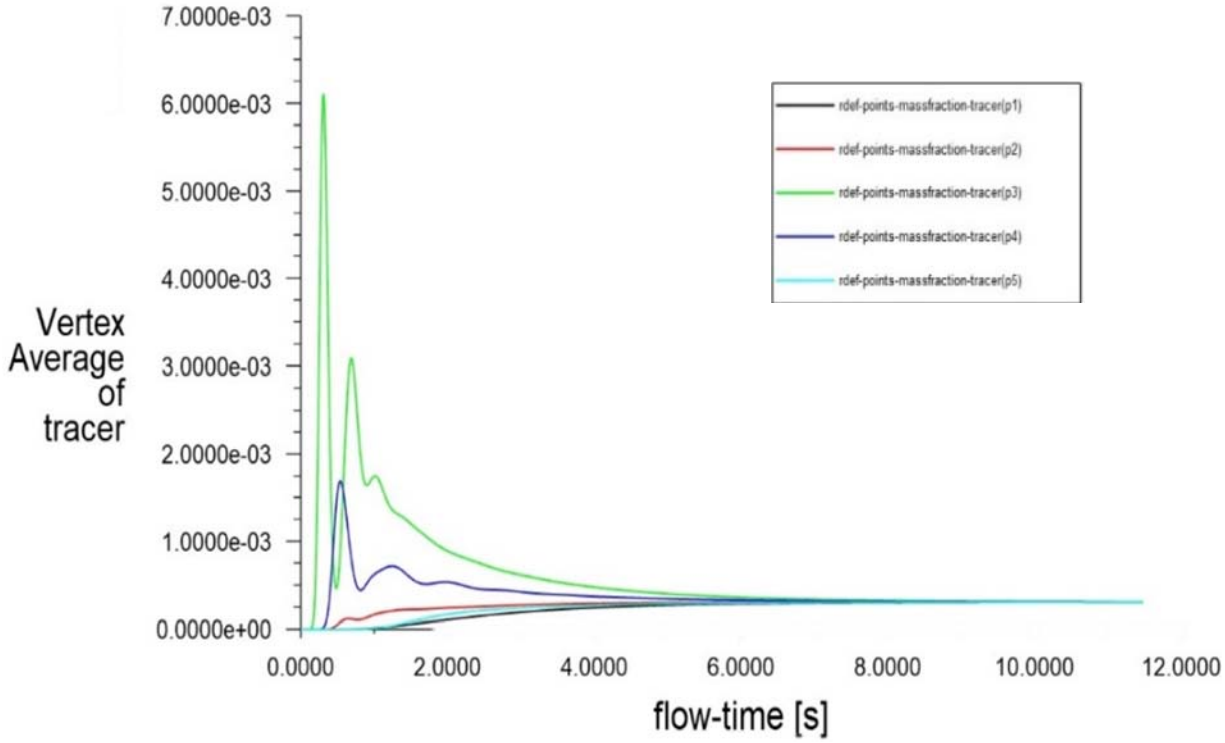

Figure 5.26: Propeller Impeller Unbaffled @ 700 RPM

5.4. Correlation between mixing time and impeller type

The time taken to complete the mixing with respect to RPM and the different impellers has been represented in the graphical manner below.

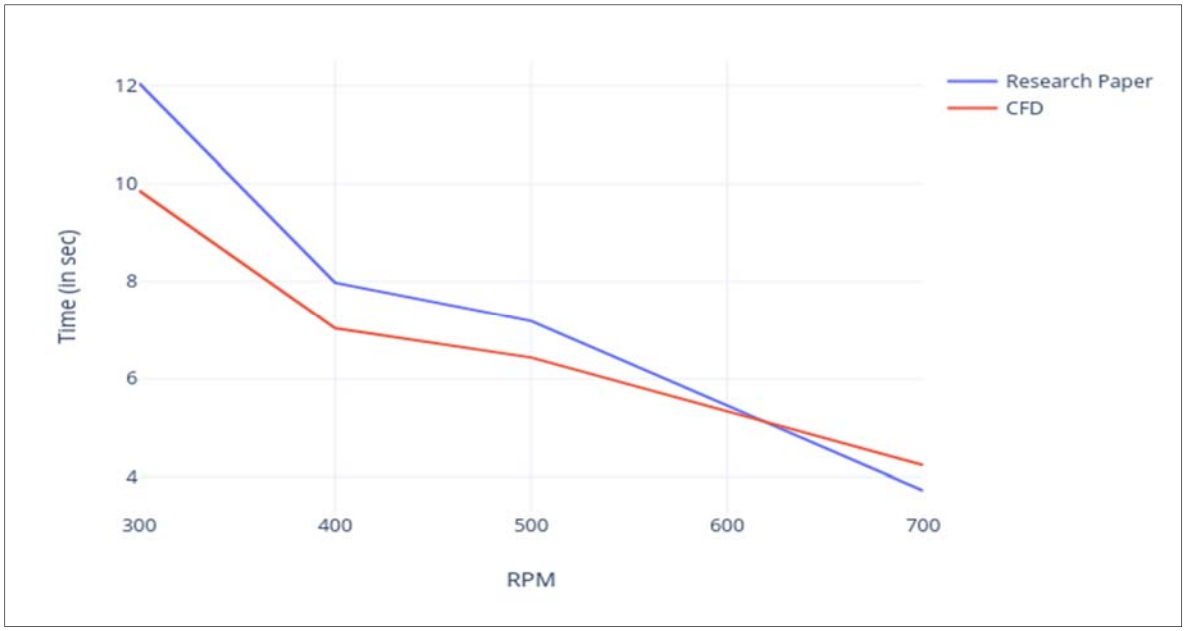

Figure 5.27: Concentration Radial Impeller Baffled

It can be observed in figure 5.27 that the calculated CFD mixing times are generally lower than the experimental mixing times from the research paper, and this trend is consistent across all speeds. However, the difference between the calculated and experimental mixing times decreases as the speed increases.

It can be observed in figure 5.28 that the calculated CFD mixing times are generally higher than the experimental mixing times, and this trend is consistent across all speeds. However, the difference between the calculated and experimental mixing times varies at different speeds. At lower speeds (300 and 400 RPM), the calculated mixing time values are much higher than the experimental values, whereas at higher speeds (500 and 700 RPM), the difference between the calculated and experimental mixing times is lower.

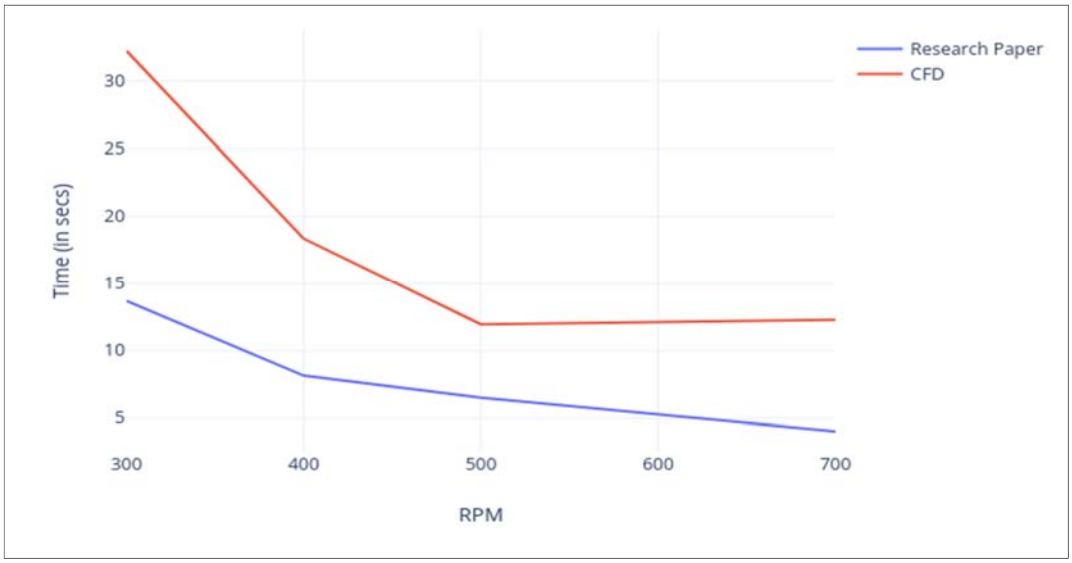

Figure 5.28: Concentration Radial Impeller Unbaffled

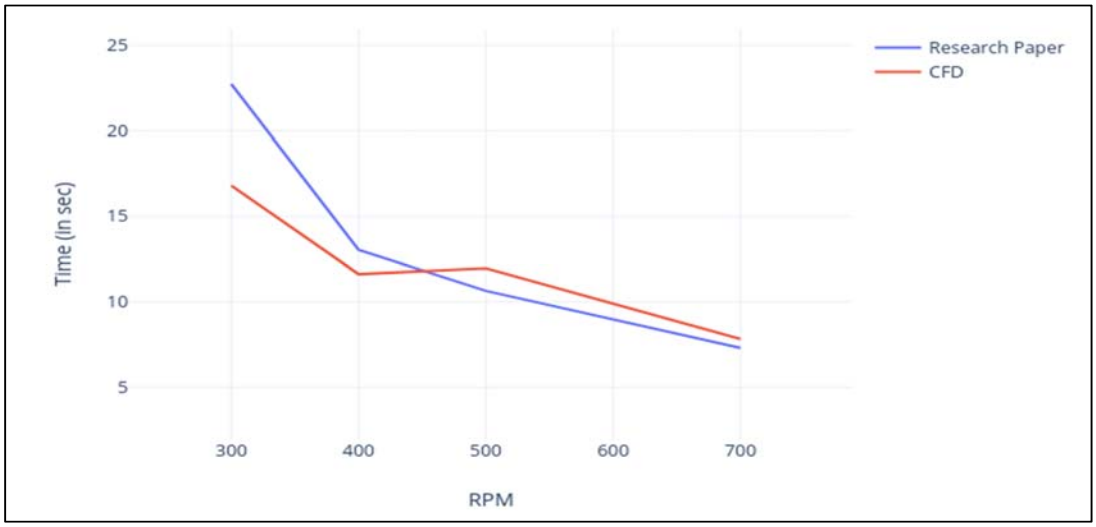

Figure 5.29: Concentration Inclined Impeller Baffled

At 300 RPM, the calculated mixing time is much lower than the experimental value, while at 400 RPM, the calculated and experimental mixing times are relatively close to each other. At 500 and 700 RPM, the calculated mixing times are higher than the experimental values.

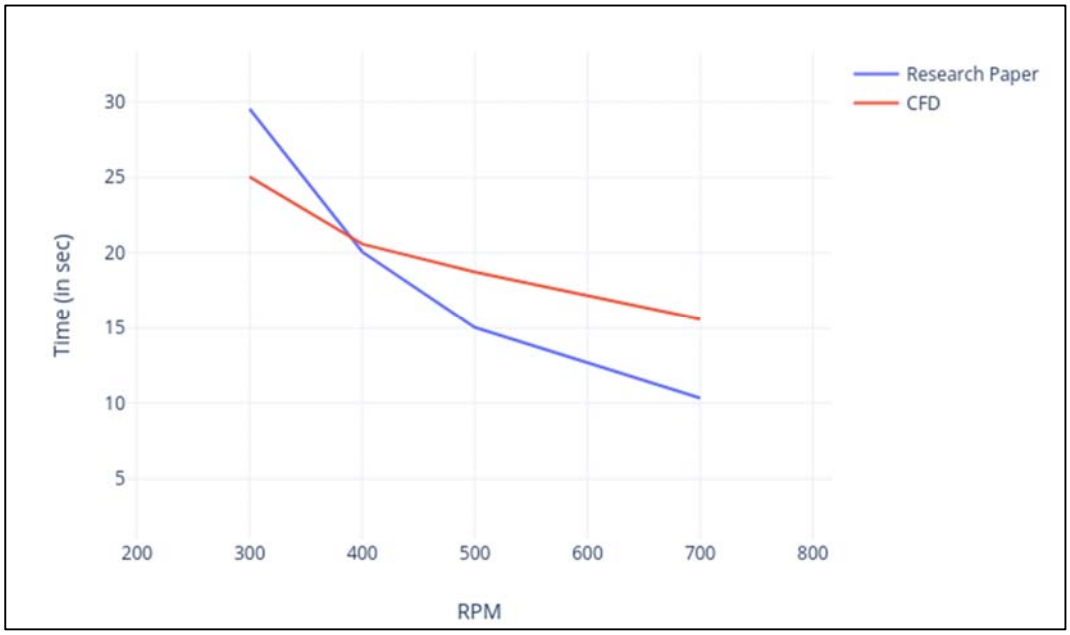

Figure 5.30: Concentration Inclined Impeller Unbaffled

It can be observed in figure 5.30 that the calculated CFD mixing times and the experimental mixing times show a mixed trend, which varies with the speed of the system. At the lowest speed of 300 RPM, the calculated mixing time is much lower than the experimental value, while at the higher speeds of 500 and 700 RPM, the calculated values are higher than the experimental values. At 400 RPM, the calculated and experimental mixing times are relatively close to each other.

It can be observed in figure 5.31 that the calculated CFD mixing times are in good agreement with the experimental mixing times, and this trend is consistent across all speeds. At all speeds, the difference between the calculated and experimental mixing times is relatively small, indicating that the CFD model used to calculate the mixing times is likely to be accurate and reliable.

It can be observed in figure 5.32 that the calculated CFD mixing times are generally higher than the experimental mixing times at all speeds, except for the second speed of 400 RPM where the experimental mixing time is much lower than the calculated mixing time. The large difference between the calculated and experimental mixing times at 400 RPM could be due to experimental errors or limitations of the CFD model used.

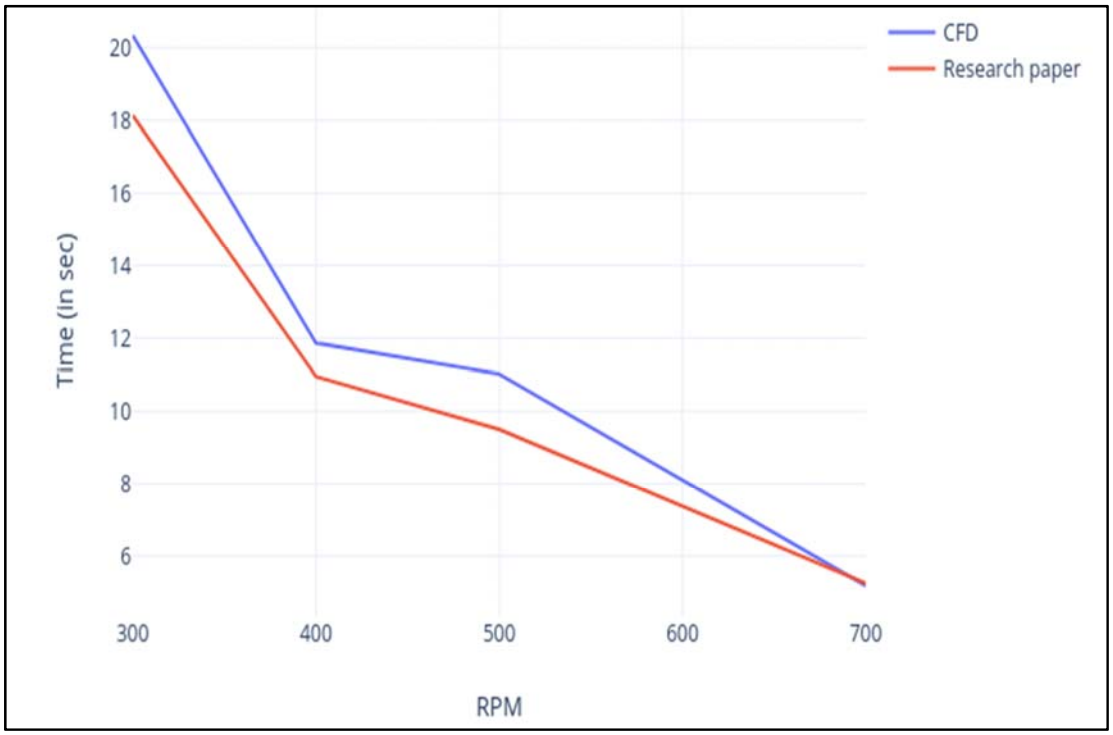

Figure 5.31: Concentration Propeller Impeller Baffled

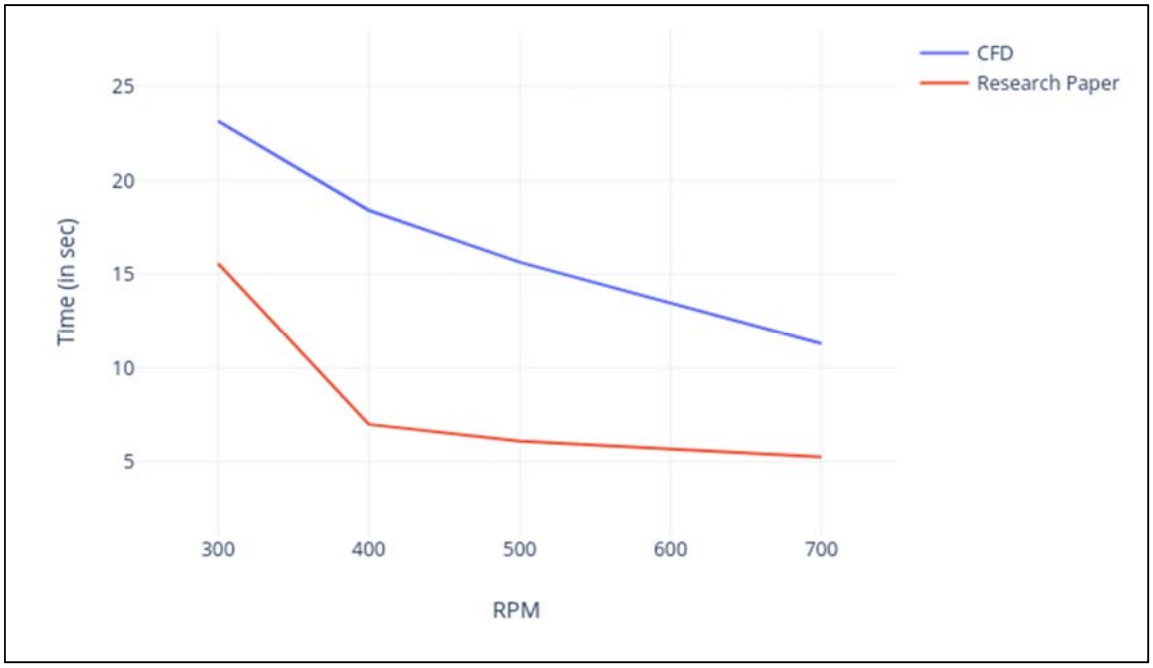

Figure 5.32: Concentration Propeller Impeller Unbaffled

5.5. Correlation between mixing time and blade angle

The time taken to complete the mixing with respect to RPM and the different angles of Inclined impeller has been represented in the table 5.1.

Table 5.1: Correlation between mixing time and blade angle

RPM		Mixing Time									
700	Parameter	Modified		Modified		Actual		Modified		Modified	
	Theta	15		30		45		60		75	
	Mixing Quality	95%	99%	95%	99 %	95%	99%	95%	99%	95%	99%
	Baffled	3.7	5.2	4.1	7.3	4.78	7.83	6.6	9.4	6.5	10
	Unbaffled	4.6	6.5	7.0	10	11.03	15.61	4.7	7.4	5.5	7.5

5.6. Correlation between mixing time and shaft clearance

The time taken to complete the mixing with respect to RPM and the different shaft clearance of Inclined impeller has been represented in the table 5.2.

Table 5.2: Correlation between mixing time and shaft clearance

RPM	Mixing Time					
700	Parameter	Modified		Modified		Actual	
	Shaft Clearance	15		27		42.52	
	Mixing Quality	95%	99%	95%	99%	95%	99%
	Baffled	5.5	8.1	8.2	10.9	4.78	7.83
	Unbaffled	9.0	12	9.6	13.1	11.04	15.61

6. Conclusion

In this project, CFD approach is taken into consideration which requires more computational resources to solve when compared to various experimental methods, but it gives more accurate solutions. In this project, a CFD methodology to simulate flow fields is developed and used in six tank-stirrer geometries. For the correct modelling of the flow fields, the realizable k-epsilon turbulence model is used, offering good results. The methodology uses the MRF approach to calculate a first initial solution, used afterwards to run a transient case. This combination of approaches allows a fast and accurate result, able to capture existing periodicities in the flow. To use this method, the domain of the tank is divided in two, a stationary and a spinning region. This project has shown how an incorrect definition of regions leads to unphysical results. It has been concluded that a good practice is to keep the spinning region close to the impeller, where there is substantial flow movement.

The selected turbulence model has worked correctly in both tank-stirrer combinations. With the help of mesh sensitivity analysis, we got a good mesh count with the help of which there was not a lot of difference from the expected solution. This project has also shown the effect of using different impeller and tank configuration. The optimal results can be found in the configuration where the radial impeller is used along with baffled configuration. But if an application requires an unbaffled configuration to be used it is better to use a propeller impeller. The effect of different angles for Inclined impellers was also studied. And it can be found that the angle has a significant effect on the mixing time. Even the effect of various shaft clearance was studied. It can be summarized that the shaft clearance should be kept around 0.33 to 0.142 times of the tank height to get an optimal solution. Furthermore, the experimentally measured mixing time was compared with the simulated time using CFD simulation, showing a good correlation between CFD predictions and measured times.

7. Future Work

One of the critical aspects of improving mixing quality is the development of more accurate and reliable definitions and metrics for assessing the quality of mixing. Mixing quality can be defined in terms of various parameters, such as homogeneity, degree of dispersion, mixing time, power consumption, and mass transfer rate. However, different definitions can lead to different results and conclusions, making it challenging to compare different mixing systems and optimize their performance.

Therefore, future work in this area could focus on developing improved definitions of mixing quality that account for various aspects of mixing, such as the flow pattern, turbulence, shear rate, and residence time distribution. For example, the mixing index can be defined as the ratio of the standard deviation of the concentration distribution to the mean concentration, which provides a measure of the degree of dispersion of the material. Other metrics, such as the mixing time, can be defined as the time required for achieving a specified level of homogeneity or degree of dispersion.

Another critical aspect of improving mixing quality is conducting a detailed experimental campaign to obtain the effect of diverse designs and operating parameters on mixing efficiency. Experiments can provide valuable insights into the fundamental mechanisms of mixing and the factors that influence mixing performance. For example, experiments can be designed to investigate the effects of impeller design, tank geometry, baffles, and other factors on mixing efficiency.

In this regard, future work could focus on conducting systematic and comprehensive experimental campaigns that cover a wide range of operating conditions and parameters. Experiments can be performed using several types of mixers, such as paddle mixers, static mixers, and jet mixers, as well as varied materials and fluids. The experimental data can be used to validate and calibrate mixing models, as well as to develop empirical correlations and design guidelines for mixing systems.

Numerical modelling is an essential tool for analysing and optimizing mixing systems, as it allows for the simulation of complex fluid flow and mixing phenomena. However, the accuracy of numerical models depends on the assumptions, simplifications, and approximations made in the model, as well as the level of detail and resolution of the computational grid.

Therefore, future work in this area could focus on exploring different modelling approaches and techniques to improve the accuracy and reliability of mixing models. For example, different turbulence models, such as the k-epsilon and k-omega models, can be used to simulate the turbulent flow and shear rate in mixing systems. Multiphase models, such as the volume of fluid (VOF) and species transport

models, can be used to simulate the mixing of two or more immiscible fluids or the chemical reactions between different components.

Different geometries for the computational grid, such as hexahedral or polyhedral cells, can be used to improve the resolution and accuracy of the simulation. The use of high-performance computing (HPC) resources can also enable more detailed and accurate simulations by reducing the computational time and increasing the spatial and temporal resolution of the simulation.

Besides the above-discussed aspects, there are several other parameters that can be explored in future work to enhance mixing quality. These parameters can be divided into two categories: physical parameters and simulation parameters.

- Physical Parameters

Physical parameters refer to the design and operating parameters of the mixing system, such as impeller design, tank geometry, baffles, and other factors. Future work in this area could focus on exploring different configurations and combinations of these parameters to optimize mixing efficiency and quality.

- Different Types of Impellers:
  Impellers play a crucial role in the mixing process by creating the necessary fluid flow and shear rate to achieve efficient mixing. However, the design and type of impeller can significantly influence the mixing performance. Future work could explore different types of impellers, such as axial flow, radial flow, and mixed flow impellers, and investigate their effects on mixing efficiency.
- Tilting the Shaft with the Impeller:
  Another aspect that can be explored is tilting the shaft with the impeller. Tilting the shaft can create a more complex fluid flow pattern and increase the shear rate, which can enhance mixing efficiency. However, this can also increase the power consumption and lead to mechanical and structural issues. Therefore, future work could investigate the optimal angle and configuration for tilting the shaft with the impeller.
- Changing the Design of the Tank's Geometry:
  The tank geometry also plays a crucial role in mixing efficiency, as it influences the flow pattern and residence time distribution of the material. Different tank geometries, such as cylindrical, conical, and rectangular tanks, can be explored to optimize mixing efficiency. Future work could

investigate the effects of tank geometry on mixing performance and develop design guidelines for optimal tank geometry.

- Removing the Hub and Fixing the Blade on the Shaft:

  One of the limitations of traditional impeller design is the presence of the hub, which can create dead zones and reduce mixing efficiency. Therefore, future work could explore the use of hub less impeller designs, where the blade is fixed directly on the shaft. Hub less impellers can improve mixing efficiency by reducing dead zones and increasing the shear rate. However, this can also increase the power consumption and lead to structural and mechanical issues.

- Increasing and Decreasing the Blade Number:

  The number of blades on the impeller also influences mixing efficiency, as it affects the flow pattern and shear rate. Different blade numbers, such as two, three, four, and six blades, can be explored to optimize mixing performance. Future work could investigate the effects of blade number on mixing efficiency and develop design guidelines for optimal blade number.

- Trying the Blade at Different Positions and Angles:

  The position and angle of the blade on the impeller can also influence mixing efficiency. Future work could explore different blade positions and angles, such as near the top, middle, or bottom of the tank, and investigate their effects on mixing efficiency. Additionally, the blade angle can be adjusted to create a more complex flow pattern and increase the shear rate, which can enhance mixing efficiency.

- Tilting the Baffles or Reducing the Number of Baffles:

  Baffles play a crucial role in preventing swirling and ensuring proper fluid flow in the tank. However, the number and position of the baffles can significantly influence mixing efficiency. Future work could explore the effects of tilting the baffles or reducing the number of baffles on mixing efficiency. Additionally, different baffle designs, such as flat, curved, or spiral baffles, can be investigated to optimize mixing performance.

- Simulation Parameters

Simulation parameters refer to the parameters and settings used in the numerical simulation of mixing systems. Future work in this area could focus on exploring different simulation parameters and techniques to improve the accuracy and efficiency of mixing models.

- More Fine Mesh:

  Increasing the mesh count can improve the resolution and accuracy of the simulation, as it allows for a more detailed representation of the fluid flow and mixing phenomena. Future work could

focus on exploring different methods for increasing the mesh count, such as using adaptive mesh refinement or parallel computing. Additionally, the effects of mesh count on the accuracy and efficiency of the simulation could be investigated to develop guidelines for optimal mesh count.

- Multiphase (VOF) Model:

  The multiphase (VOF) model is a technique used to simulate the interaction between separate phases in a mixing system, such as gas and liquid or two immiscible liquids. This model can improve the accuracy and realism of the simulation by accounting for the effects of multiphase flow on mixing efficiency. Future work could explore the use of the VOF model in mixing simulations and investigate its effects on the accuracy and efficiency of the model.

- Different Shapes for Patching:

  The accuracy and efficiency of the mixing simulation can also be improved by using different shapes for patching, such as hexagonal or triangular shapes. These shapes can provide a more efficient representation of the fluid flow and mixing phenomena and improve the accuracy of the model. Future work could investigate the use of different patching shapes in mixing simulations and compare their effects on the accuracy and efficiency of the model.

8. Bibliography

[1] Ingham J., Dunn I. J., Heinzle E., Prenosil J.E., Snape J.B. (2007), Chemical Engineering Dynamics, WILEY-VCH

[2] Danckwerts P.V. (1952), The definition and measurement of some characteristics of mixtures, Appl. Sci. Res. A3:279-296.

[3] Paul L.P., Atieno-Obeng V.A., Kresta S.M. (2004), Handbook of Industrial Mixing, Wiley-Interscience.

[4] Kukukova A., Aubin J., Kresta S. (2009), A new definition of mixing and segregation: Three dimensions of a key process variable, Chem. Eng. Res. Des. 87:633-647. doi: 10.1016/j.cherd.2009.01.001.

[5] Distelhoff M.F.W., Marquis A.J., Nouri J.M., Whitelaw J.H. (1997), Scalar mixing measurements in batch operated stirred tanks. Can. J. Chem. Eng. 75:641–652. doi:10.1002/cjce.5450750401

[6] Kramers H., Baars G.M., Knoll W.H. (1953), A comparative study on the rate of mixing in stirred tanks. Chem. Eng. Sci. 2:35-42. doi:10.1016/0009-2509(53)80006-0.

[7] Grenville R.K. (1992), Blending of Viscous Newtonian and Pseudo-Plastic Fluids, Ph.D. dissertation, Cranfield Institute of Technology, Cranfield, Bedfordshire, England.

[8] Khang S.J., Levenspiel O. (1976), New Scale Up and Design Method for Stirrer Agitated Batch Mixing Vessels. Chem. Eng. Sci. 31:569. doi:10.1016/0009-2509(76)80020-6.

[9] Bakker A. (2006), Blend Times in Stirred Tanks: Reacting Flows - Lecture 9, available at http://www.bakker.org/dartmouth06/engs199/09-blend.pdf (accessed 11 October 2015).

[10] Ghotli A.R., Raman A.A.A., Ibrahim S., Baroutian S. (2013). Liquid-liquid mixing in stirred vessels: A review. Chem. Eng. Commun. 200:595–627. doi:10.1080/00986445.2014.938805.

[11] Nere N.K., Patwardhan A.W., Joshi J.B. (2003). Liquid-Phase Mixing in Stirred Vessels: Turbulent Flow Regime. Ind. Eng. Chem. Res. 42, 2661–2698. doi:10.1021/ie0206397.

[12] Dragan D. N., Giuseppe C., Patrick J. F. (2016), Mixing Time—Experimental Determination and Applications to the Modelling of Crystallisation Phenomena, doi:10.20944/preprints201611. 0022.v1

[13] A. Delafosse, J. M. (2009). Trailing vortices generated by a Rushton turbine: Trailing vortices generated by a Rushton turbine: Chemical Engineering Research and Design, 401-411.

[14] Cahill, J. D. (2009). Laminar flow. Retrieved from UNM Physics and Astronomy: https://www.youtube.com/watch?v=p08_KlTKP50&ab_channel=UNMPhysicsandAstronomy

[15] D. Ankamma Rao, P. S. (2008). Experimental and CFD simulation studies on power consumption in mixing using energy saving turbine agitator. Journal of Industrial and Engineering Chemistry, 159-161.
[16] Harminder Singh, D. F. (2011). An assessment of different turbulence models for predicting flow in a baffled tank stirred with a Rushton turbine. Chemical Engineering Science, 5976-5988.
[17] Harshal Patil, A. K. (2018). CFD simulation model for mixing tank using multiple reference frame (MRF) impeller rotation. ISH Journal of Hydraulic Engineering, 1-10.